Lawrence Berkeley National Laboratory
LBL Publications

Title
Nanostructured Ferroelectric-Polymer Composites for Capacitive Energy Storage

Permalink
https://escholarship.org/uc/item/1zx358cg

Journal
Small Methods, 2(6)

ISSN
2366-9608

Authors
Li, He
Liu, Feihua
Fan, Baoyan
et al.

Publication Date
2018-06-01

DOI
10.1002/smtd.201700399

Peer reviewed

eScholarship.org Powered by the California Digital Library
University of California

WILEY-VCH

DOI: 10.1002/ ((please add manuscript number))
Article type: Review

Nanostructured Ferroelectric Polymer Composites for Capacitive Energy Storage

*He Li, Feihua Liu, Baoyan Fan, Ding Ai, Zongren Peng, and Qing Wang**

H. Li, Prof. Z. Peng
State Key Laboratory of Electrical Insulation and Power Equipment, School of Electrical Engineering, Xi'an Jiaotong University, Xi'an 710049, China

H. Li, F. Liu, B. Fan, D. Ai, Prof. Q. Wang
Department of Materials Science and Engineering, The Pennsylvania State University, University Park, PA 16802, USA
E-mail: wang@matse.psu.edu

Keywords: Ferroelectric Polymers, Nanocomposites, Inorganic Nanostructures, Energy Storage, Capacitors,

The introduction of inorganic components into polymer matrix to form polymer composites is an emerging and promising approach to dielectric materials for capacitive energy storage. Ferroelectric polymers are particularly attractive as matrices for dielectric polymer composites owing to their highest dielectric constant (≥10) among the known polymers. In this review article, we summarize the important aspects and recent advances in the development of the ferroelectric polymer based dielectric polymer composites for high energy density capacitor applications. This overview describes the preparation methods of ferroelectric polymer composites with zero-, one- and two-dimensional nanostructured fillers, the surface-modified nanofillers and hierarchically structured fillers, and their comprehensive impacts on the dielectric properties, breakdown strength, and energy density of the resulting composites. The

most recent progress on the incorporation of multiple nanofillers with complementary functionalities into ferroelectric polymers and the design of layer-structured ferroelectric polymer composites have also been highlighted. This review concludes with a discussion of scientific and technological issues that remain to be addressed as well as an outlook for the future of ferroelectric polymer-based dielectric composites.

1. Introduction

With the rapid development of science and technology, ever-increasing demand has been created for high-performance energy storage devices in advanced electronics, electric vehicles, and power systems, et al.[1, 2] At present, with increasing consumption of fossil resources, the evolution in "green" energy has become an inevitable choice for the sustainable development. However, the storage and conversion of these decentralized, unstable, intermittent energy sources including wind, solar, tidal energies is a challenging issue.[3–5] Among various electrical energy storage devices including batteries, supercapacitors and film capacitors, batteries demonstrate high energy densities via storing the electricity in the form of chemical energies, however, it is difficult to offer high power density to meet the demand in rapid charge–discharge applications.[6–9] Supercapacitors exhibit higher power densities and long cycling lifespans, but are limited by the chemical and electrochemical stability of the electrolytes, as well as a relative low operating voltage.[10–13]

Polymer film capacitors possess the advantages of low cost, facile fabrication, excellent flexibility, and high operating voltage, which display the highest power

densities in comparison with batteries and supercapacitors and are widely used in electronic devices and power systems.[14–18] Although the state-of-the-art capacitor film represented by biaxially oriented polypropylene (BOPP) exhibits ultra-high charge–discharge efficiency, the energy density has been significantly limited by its low dielectric constants (K), which is only about 1–2 J cm^{-3}.[19] To address this issue, ferroelectric polymers represented by poly(vinylidene fluoride) (PVDF) and its copolymers and terpolymers with relatively high K (≥10) have been regarded as the most promising polymeric materials for high-energy-density film capacitors.[16–23] More importantly, since capacitors can contribute more than 25% of the volume and weight to the electric power systems, the dramatic improvement of energy density of film capacitors would help to reduce the volume, weight and cost of electronic devices and hybrid electric vehicles, et al.[24, 25]

The K value of ferroelectric polymers, however, is still considerably low in comparison with those of ceramic dielectrics (e.g., K of 10^4–10^5) for capacitive energy storage, though these ceramics suffer from low dielectric breakdown strength (E_b) and poor scalability.[26–29] Thus, a composite approach has been developed to improve energy storage capability via introducing high K inorganic fillers into ferroelectric polymers with high E_b and facile processability. For the dielectric polymer nanocomposites, the total stored energy densities, which are the sum of the energy densities of the ceramic filler and the polymer phases, are derived from $U_d = f_1U_d^{(1)} + f_2U_d^{(2)} + gU_d^{(3)}$, where U_d is energy density, f_1 is volume fraction of ceramic filler, f_2 is volume fraction of polymer matrix and g is interfacial area between filler and polymer.

As ferroelectric polymers have the highest energy densities among the known dielectric polymers, they have been considered as the material of choice as polymer matrix candidates for dielectric polymer nanocomposites. Moreover, relatively high K values of ferroelectric polymers help to alleviate local field distortion in the composites caused by a large mismatch in K values between fillers and polymer matrixes.[30–32] The presence of highly inhomogeneous electric field leads to a significantly reduced effective E_b of the dielectric polymer nanocomposites.

2. Dielectrics for Capacitive Energy Storage

Capacitive energy storage in dielectrics, which is a physical process in essence, involves no chemical reactions, that is, the charge moves inside the dielectrics under the applied electric field, resulting in the electric displacement to store energy.[2, 16] In general, the energy density (U_d) of a dielectric can be expressed by $U_d = \int E\mathrm{d}D$, where E is applied electric field and D is electric displacement.[17] For a linear dielectric such as BOPP, whose relative dielectric constant is independent on the applied electric field, the energy density can be expressed by $U_d = 1/2DE = 1/2K\varepsilon_0E^2$, where D is electric displacement, E is applied electric field, K is relative dielectric constant, and ε_0 is the vacuum dielectric constant (8.85×10^{-12} F m^{-1}). As seen in the equation for linear dielectrics, the two factors that affect the energy density are relative dielectric constant (K) and electric field strength. Note that, as the energy density is proportional to the square of the applied electric field, it is largely determined by the E_b of dielectrics.[33]

The discharged energy density can be calculated from the electric displacement–

electric field *D–E* hysteresis loops by the integral of the shaded area bounded by the discharging curve. **Figure 1**a and 1b show the unipolar *D–E* loops for both linear and nonlinear dielectrics. For ferroelectric materials, the bipolar *D–E* loop for a dielectric with normal ferroelectric behavior is shown in Figure 1c, the bipolar *D–E* loops for dielectrics with relaxor ferroelectric and antiferroelectric behaviors are shown in Figure 1d and 1e, respectively.[34] The energy density that can be released from dielectrics (shaded area), i.e. discharged energy density, can be largely reduced as a result of ferroelectric loss, which is associated with remnant polarization arisen from irreversible dipoles.[16, 35]

Note that the charged energy density is not equal to the discharged energy density especially for the ferroelectric materials. In this article, we refer the energy density to the discharged energy density in the following sections. It is agreed that not only the energy density but also the charge–discharge efficiency of dielectrics should be equally considered as key performance parameters for capacitors. The charge–discharge efficiency can be derived from $\eta = U_d/U_c$, where η is charge–discharge efficiency, U_c is charged energy density, and U_d is discharged energy density.[35] The electrical energies that can not be released from dielectrics is usually converted into waste heat, which can lead to film aging and even cause catastrophic failure of capacitors.[36, 37] Therefore, the charge–discharge efficiency is an important indicator for ferroelectric polymers in capacitive energy storage applications.

3. Ferroelectric Nanocomposites for Capacitive Energy Storage

The ferroelectric fluoropolymers including PVDF, PVDF-based copolymers and terpolymers exhibit high K values (≥ 10) and have been extensively studied for capacitive energy storage. The efforts have been focused on the structural modification of ferroelectric fluoropolymers, namely, by adjusting the microstructure of the polymers via physical and chemical means to improve K, reduce ferroelectric loss, and increase E_b to ultimately achieve high energy densities.

PVDF is one of the most extensively used fluoropolymers, which contains ~59.4 wt% fluorine atoms with a density of ~1.75 g cm^{-3}.[38] Due to the significant different electronegativity between fluorine atoms and hydrogen atoms, there exhibits a large number of intrinsic dipole moments in the PVDF molecular chains, which leads to a high K.[16] **Figure 2** shows three major crystal forms of PVDF, including *trans-gauche* conformation (TGTG') for α-phase, all *trans* planar zigzag conformation (TTTT) for β-phase, and three *trans* linked to *gauche* (TTTG) for γ-phase.[39, 40] Note that δ-phase is a polar version of the α-phase.[39, 40] Among different conformations in PVDF, α-phase is nonpolar with the dipole moments canceling out each other and exhibits a kinetic steady state, while β-, γ- and δ-phases exhibit high polarizability due to the presence of net dipole moments.[41–43] In particular, β-phase has the highest dipole moment in perpendicular to chain length, which exhibits a thermodynamically steady state with excellent ferroelectric, piezoelectric and pyroelectric properties.[44] At low applied electric fields, PVDF in α-, β- and γ-phases display little difference in energy storage and loss properties. The PVDF in β-phase exhibits the lowest energy density (i.e. 1.5 J cm^{-3} at 150 MV m^{-1}) due to the premature saturation of polarization.[40] For the

quenched PVDF, *α*-phase in PVDF can be transformed to *γ*-phase at the electric field of 200–350 MV m^{-1}. The *γ*-phase in PVDF is much more stable at high electric fields, which gives rise to a high energy density of ~14 J cm^{-3} at 500 MV m^{-1}.[40]

To improve the capacitive properties of PVDF, structural defects were introduced into the molecular chains of PVDF to yield the ferroelectric polymers with relaxor behaviors.[23, 45, 46] Poly(vinylidene fluoride-*co*-trifluoroethylene) (P(VDF-TrFE)) copolymers have been widely used in the applications of sensors and actuators since their excellent ferroelectric behavior has been found.[47] However, the introduction of TrFE into PVDF also restrains the formation of gauche bond and thereby stabilizes the *β*-phase, which destines its premature saturation of polarization and low discharged energy density.[48] To change its relaxation behaviors, high energy radiation was utilized to modify P(VDF-TrFE),[45–52] which affects both physical and chemical structures of polymers, e.g., chain scission, bond rearrangements and crosslinking reactions.[53–55] Chu et al. reported a PVDF-based copolymer which was synthesized by copolymerization of VDF with chlorotrifluoroethylene (CTFE).[23] Following this work, Zhou et al. fabricated a biaxially oriented P(VDF-CTFE) (91/9 mol%) copolymer under a low saturation polarization field, which exhibits a high energy density of ~25 J cm^{-3} at 600 MV m^{-1}.[46] Furthermore, Wang and coworkers chemically crosslinked P(VDF-CTFE) from the Cl sites in the polymer chains, a maximal energy density of ~17 J cm^{-3} at 400 MV m^{-1}, along with a high charge–discharge efficiency of 83% is achieved.[56] The cross-linked network in the polymer restricts the chain mobility and generates deep traps to reduce the conduction loss, and the cross-linked structure also enhances the

reversibility of crystalline dipole switching in that which helps to pull the aligned dipoles back to the original nonpolar conformation during discharging, resulting in a lower ferroelectric loss.[56–58] Similar to the introduction of CTFE into PVDF chains, hexafluoropropylene (HFP) was also employed as a monomer in the copolymerization with VDF.[59, 60] P(VDF-HFP) shows comparatively lower crystallinity than PVDF due to the presence of bulky CF_3 groups. The ferroelectric properties of P(VDF-HFP) are strongly dependent on different fabrication conditions, e.g., solution casting, hot pressing and stretching.[61] Consequently, P(VDF-HFP) (96/4 mol%) copolymers fabricated from different methods exhibit energy densities varying from 11 to 13.5 J cm^{-3} at ~600 MV m^{-1}.[59] More recently, poly(vinylidene fluoride-*co*-bromotrifluoroethylene) P(VDF-BTFE) copolymers were synthesized by Gadinski et al.[62] A very high energy density of ~20.8 J cm^{-3} is achieved in P(VDF-BTFE) (95/5 mol%) copolymer at 716 MV m^{-1}.

In addition to the electron beam irradiation approach to induce relaxor ferroelectric behaviors from P(VDF-TrFE), structural defects from a third comonomer including CTFE, HFP, chlorofluoroethylene (CFE), chlorodifluoroethylene (CDFE), and trifluoropropene (TFP) have been introduced into the molecular chains of P(VDF-TrFE) to achieve novel ferroelectric behaviors in the PVDF-based terpolymers.[63–72] It is reported by Zhang et al. that K of P(VDF-TrFE-CTFE) (65.6/26.7/7.7 mol%) terpolymer reaches up to ~60 (at 1 kHz) at its Curie temperature (35–40 °C). An energy density of ~13 J cm^{-3} is obtained at its E_b of ~500 MV m^{-1}.[73] For P(VDF-TrFE-CFE) terpolymer, the randomly oriented CFE offers temporary physical pinning to P(VDF-

TrFE) chains due to the small size and large dipole moment, which affects the chain conformation, crystal phase, and crystallite size et al.[74] It is reported by Chu et al. that an energy density of ~9 J cm^{-3} at the breakdown field of 400 MV m^{-1} is obtained in the P(VDF-TrFE-CFE) (63/37/7.5 mol%) terpolymer.[75]

With the development of nanotechnology in recent decades, a composite approach has been developed to improve dielectric properties and energy storage capabilities of ferroelectric polymers via introducing high *K* of inorganic nanofillers into polymer matrix to yield the dielectric polymer nanocomposites. However, the dispersion of inorganic nanofillers in ferroelectric polymers is always challenging due to the high surface energy of nano-sized fillers as well as the very different physical and chemical surface properties between nanofillers and fluoropolymer matrix. As a result, agglomeration happens, which may introduce a large number of defects into nanocomposites and also give rise to electron conduction for high dielectric loss and undesirable porosity for E_b at much lower fields.[2, 76] Therefore, surface modification is highly needed in most cases to reduce the agglomeration of fillers and improve the compatibility between fillers and polymer matrix, thereby reducing the dielectric loss and improving the E_b as well as the energy density of nanocomposites.[76, 77] The surface modification processes for nanofillers are described and discussed in detail in Section 3.1.1 and 3.1.2.

In this section, we summarize the rational design, preparation methods, dielectric properties and capacitive performance of nanostructured dielectric composites using PVDF-based ferroelectric polymers. The nanostructured ferroelectric polymer

composites can be mainly divided into three strategies: the two-phase nanocomposites based on nano-sized fillers including the surface modification of fillers, the nanocomposites with heterogeneous filler compositions, and the nanocomposites based on hierarchically structured nanofillers. They are described and discussed in detail below.

3.1. Two-Phase Ferroelectric Nanocomposites

In recent decades, the ferroelectric polymer-based nanocomposites have been prepared using different kinds of nanofillers, which can be divided into three categories according to filler morphologies: 1) Spherical (zero-dimensional) filler: Fillers that are in nanoscale in all three dimensions. In dielectric polymer nanocomposites, the nanoparticles with relatively low *K* such as silicon dioxide (SiO_2), zirconium dioxide (ZrO_2), aluminium oxide (Al_2O_3) and magnesium oxide (MgO) have been widely selected as insulating barriers to resist dielectric breakdown and reduce leakage current.[78–82] Besides, the ferroelectric ceramic nanoparticles with higher *K* such as barium titanate (BT) and brium strontium titanate (BST),[83–86] have also been used to increase the *K* and then improve the energy storage capacity of the nanocomposites. 2) One-dimensional filler: Fillers that are in nanoscale in two dimensions. Carbon nanotube (CNT) is the most commonly used one-dimensional filler in polymer nanocomposites to improve dielectric constant.[87, 88] In addition, boron nitride nanotubes[89] and ceramic nanowires and/or nanofibers such as titanium dioxide (TiO_2), BT and BST have been incorporated into the ferroelectric polymer matrix.[90–92] 3) Two-

dimensional filler: Fillers that are in nanoscale in only one dimension. Graphene oxide (GO) nanosheets,[93] molybdenum disulfide (MoS_2) nanosheets,[94] montmorillonite (MMT) nanoplatelets[95, 96] as well as boron nitride (BN) nanosheets[97, 98] et al. have been selected as two-dimensional fillers in the ferroelectric polymer nanocomposites.

3.1.1. Nanocomposites Based on Spherical Fillers

Among various spherical fillers (particles), ferroelectric ceramic nanoparticles, especially $BaTiO_3$, have been frequently used. Dang et al. evaluated the effects of nanoparticle size on the dielectric properties of the PVDF/BT composites.[83] The composites with the BT nanoparticles in average diameter of 50–80 nm exhibits the highest K in comparison with 30–50 nm and 100–150 nm sized BT based nanocomposites. The result could be explained by the interfacial polarization and the different crystal phases of BT nanoparticles. To achieve a uniform dispersion of fillers, hydrogen peroxide (H_2O_2) was used to modify the surface of crude BT nanoparticles.[84] The surface hydroxylated-modified BT (h-BT) particles results in homogeneous morphology (**Figure 3**a), an improved E_b and a reduced loss tangent of the PVDF/BT nanocomposites, which are attributed to the hydrogen bonds formed between the fluorine atoms in PVDF and the hydroxyl groups on the surface of h-BT (Figure 3b). Compared with the nanocomposites filled with unmodified BT, the dielectric parameters of PVDF/h-BT nanocomposites are found to be much stable with temperature as well as frequency, which is attributed to the restricted movement of side groups and polymer chains near the interface between BT nanoparticles and PVDF matrix. In addition, silane coupling agent was used to modify the surface of nanofillers

to establish the interaction between fillers and polymer matrixes.[99, 100] For example, Yu et al. used silane coupling agent (NXT105) as a bridge-linked action in order to improve the compatibility between BT nanoparticles and polymers.[101] For the nanocomposite with 20 vol% BT, the electric displacement is increased to ~6.28 μC cm^{-2} in comparison with ~3.5 μC cm^{-2} for pristine PVDF at 200 MV m^{-1}, along with an energy density reaches up to ~3.54 J cm^{-3}, which is attributed to the increase in interface areas and the enhanced Maxwell−Wagner−Sillars (MWS) polarization under the applied field. Besides, Li et al. demonstrated a chemical modification method for BT nanoparticles using ethylene diamine moieties.[102] The organic chains on the BT surface not only promote the dispersibility of the particles in organic solvents but also render the particles a homogeneously distribution in both P(VDF-CTFE) and P(VDF-TrFE-CTFE) matrix. The *K* of the polymer nanocomposites increases steadily with increasing BT content. The nanocomposites based on the terpolymer with a higher *K* of ~42 at 1 kHz exhibit larger electric displacements than that of the copolymer with a *K* of ~12 under the same electric field, thereby leading to higher energy densities. For example, at 150 MV m^{-1}, the stored energy density is ~7.0 J cm^{-3} for the P(VDF-TrFE-CTFE) nanocomposite with 30 vol% BT and ~3.7 J cm^{-3} for the P(VDF-CTFE) nanocomposite with 23 vol% BT, which are ~120% and nearly two-fold enhancement in comparison with the pristine terpolymer of ~3.2 J cm^{-3} and pristine copolymer of ~1.9 J cm^{-3}.

As a mussel-inspired protein, dopamine (DOPA) and other polyphenol compounds have attracted growing attention owing to their outstanding adhesion offered by

catechol compounds, which have been employed as efficient binders for the surface functionalization of inorganic fillers.[103, 104] The amino groups and hydroxyl groups in DOPA can build a strong binding force with the polymer matrix to improve the compatibility between nanoparticles and ferroelectric polymer matrix.[105] For example, Lin et al. prepared the PVDF composites with covalently bonded dopamine modified BT (DOPA-BT) nanoparticles.[106] At 1 kHz, the nanocomposite with 50 wt% DOPA-BT exhibits a K of ~56.8 and a low loss tangent of ~0.04 in comparison with corresponding values of ~40 and ~0.2 of unmodified BT/PVDF nanocomposite. Phosphonic acid has also been employed as a surfactant to effectively improve the dispersion of BT nanoparticles in ferroelectric polymers.[107, 108] For example, 2,3,4,5,6-pentafluorobenzyl phosphonic acid (PFBPA) functionalized BT (PFBPA-BT) was employed to prepare the P(VDF-HFP)/BT nanocomposites by Kim et al.[107] The PFBPA functionalized nanocomposites at a 50 vol% filler loading exhibits a K of ~37, a loss tangent of ~0.07, a E_b of ~210 MV m^{-1}, and an energy density of ~6.1 J cm^{-3}. The PFBPA serves as a passivation layer on the BT surface guarantees the uniform dispersion of nanoparticles and reduces the trap charges, and thus yields the improvements of E_b and energy density. The authors extended their studies for P(VDF-HFP)/PFBPA-BT nanocomposites with high volume fractions of nanoparticles.[108] The measured K of the nanocomposites with low volume fractions (< 50%) is in good agreement with standard theoretical models, with a maximal K of ~35. However, for the nanocomposites with higher BT volume fractions (> 50%), the K is found to decrease with increasing filler volume fraction, e.g., from ~31 at 60 vol% to ~19 at 80

vol % loading measured at 1 kHz. A measured energy density of ~3.2 J cm^{-3} at 164 MV m^{-1} is obtained when the filler volume fraction is increased to 50%.

Nanostructured filler with core-shell structure is considered as an effective route to the organic-inorganic hybrid composites with homogeneous nanostructures owing to a significant improvement of the compatibility between nanofillers and polymer matrix.[109, 110] Yu et al. synthesized the PVDF composites via the incorporation of BT nanoparticles with a polyvinylprrolidone (PVP) shell.[111] For the nanocomposite with 55 vol% BT@PVP, a high *K* of ~77 along with a low loss tangent of ~0.05 is obtained at 1 kHz. The PVP shell helps to improve the compatibility between BT nanoparticles and polymer matrix, thus preventing the particles from aggregation in PVDF. A E_b of ~336 MV m^{-1} and an energy density of ~6.8 J cm^{-3} are obtained in the nanocomposite with 10 vol% BT@PVP loading, which is ~38% higher and nearly two times larger than those of unmodified PVDF/BT nanocomposites at the same loading, respectively. Interestingly, Jiang and coworkers synthesized core-shell structured BT nanoparticles with different shell thicknesses and different molecular structures of the shell by grafting fluoroalkyl acrylate monomers via surface-initiated reversible addition-fragmentation chain transfer (RAFT) polymerization.[112] The BT nanoparticles functionalized by poly(1H,1H,2H,2H-heptadecafluorodecyl acrylate) with long side groups and poly(trifluoroethyl acrylate) with short side groups are marked as BT@PHFDA and BT@PTFEA, respectively. It is found that the P(VDF-HFP) nanocomposites filled with BT-PTFEA with a thick fluoro-polymer shell exhibit the best dielectric properties among all the nanocomposites, whose loss tangent shows a

continuous decrease with increasing filler loading. The nanocomposite with 50 vol% BT@PTFEA (thick shell) exhibits a E_b of ~182.6 MV m^{-1} and a theoretical maximal energy density of ~6.23 J cm^{-3}, which is 50% higher than that of pristine P(VDF-HFP). Following this work, they grafted three different monomers, i.e. methyl methacrylate (MMA), hydroxyethyl methacrylate (HEMA), and glycidyl methacrylate (GMA) to the surface of BT nanoparticles to yield core-shell structures (BT@PMMA, BT@PHEMA, and BT@PGMA) via RAFT polymerization, as shown in **Figure 4**. Note that all the PVDF nanocomposites with these three types of core-shell structured BT@polymer nanoparticles are in homogeneous morphologies.[113] The dielectric properties are highly affected by the properties of the polymer shells, e.g., E_b varies from shell structures and nanoparticle loadings. The energy densities of the nanocomposites with 20 vol% BT@PHEMA, BT@PMMA, and BT@PGMA particles are ~2.18, ~2.24, and ~2.4 J cm^{-3} at 140 MV m^{-1}, respectively.

In addition to organic shell layer for nanofillers, inorganic oxide shells including SiO_2, TiO_2 and Al_2O_3 have been employed to surface-functionalize high K ceramic nanofillers.[114–116] For example, an inorganic-inorganic core-shell structure with SiO_2 coating on the surface of BT (BT@SiO_2) nanoparticles, was reported by Yu et al.[114] It is found that the SiO_2 shell serves as an insulting barrier to yield the reduction in carrier mobility and remnant polarization, thus decreases the loss tangent in the PVDF/BT@SiO_2 nanocomposites. The PVDF composite with 2 vol% BT@SiO_2 nanoparticles exhibits an E_b of ~340 MV m^{-1}, along with an energy density of ~6.28 J cm^{-3}, in comparison with the PVDF/BT particle nanocomposite with an energy density

of ~5.68 J cm^{-3} at the same filler loading. Similar to SiO_2-coated shells, TiO_2 has also been utilized as the shell layer for BT to function as a buffer between fillers and PVDF-based ferroelectric polymers, which show advantages to reduce the local distortion of electric field in the nanocomposites. Rahimabady et al. reported a high *K* of ~110 from the P(VDF-HFP) nanocomposite with 50 vol% BT@TiO_2, which is more than 3 times higher than that of the P(VDF-HFP)/BT nanocomposite at the same loading.[115] A high energy density of ~12.2 J cm^{-3} is achieved from the P(VDF-HFP)/BT@TiO_2 nanocomposite at an electric field of 340 MV m^{-1}. These improvements are attributed to the MWS interfacial polarization as a result of space charge accumulation and formation of Gouy–Chapman–Stern layers at the highly interactive interfaces in the nanocomposites. More interestingly, Yang et al. designed a strawberry-like BT@PDA-Ag hybrid nanoparticle by decorating Ag nanodots onto a core-shell polydopamine (PDA) coated BT nanoparticle (**Figure 5**a and 5b) to prepare the P(VDF-HFP)/BT@PDA-Ag nanocomposites.[117] It is found that the PDA shell not only facilitates a homogeneous dispersion of the BT nanoparticles in the polymer matrix, but also enhances the interfacial adhesion between nanofillers and polymer matrix. The super-small sized Ag dots, which are uniformly distributed on the PDA shell, successfully introduce the Coulomb–blockade effect to the nanocomposites, which inhibits the electron migration in the nanocomposites and suppresses the space charge accumulation at the nanofiller/polymer interface. The P(VDF-HFP)/BT@PDA-Ag nanocomposites exhibit higher energy densities and greater efficiencies in comparison with the composites filled with BT and BT@PDA nanoparticles (Figure 5c), e.g., an

energy density of ~3.21 J cm^{-3} is achieved at 140 MV m^{-1} in the P(VDF-HFP)/BT-PDA-Ag nanocomposite at 20 vol% loading, vs. ~2.45 J cm^{-3} for the P(VDF-HFP)/BT nanocomposite and ~2.72 J cm^{-3} for the P(VDF-HFP)/BT@PDA nanocomposite at the same filler loading.

To prevent nanoparticles from aggregation and increase their dispersibility in nanocomposites via strong and stable chemical interaction, Jiang et al. presented an organic-inorganic nanocomposite comprising monodisperse BT nanoparticles directly tethered with PVDF by capitalizing on an rationally designed amphiphilic star-like diblock copolymer as nanoreactors.[118] The amphiphilic unimolecular star-like poly(acrylic acid)-block-poly(vinylidene fluoride) PAA-*b*-PVDF diblock copolymer is synthesized by a combination of atom transfer radical polymerization (ATRP) and click reaction, followed by hydrolysis. The homogeneous PVDF/BT nanocomposites are fabricated by hot-pressing the chemically synthesized nanocomposites powder under high temperatures and pressure. Interestingly, the PVDF/BT nanocomposite with ~16 nm particles at 84.7 wt% loading exhibits a high K of ~85 (at 2 MHz) and a low loss tangent of ~0.028, in comparison with the K of ~10 and loss tangent of ~0.16 for pristine PVDF. The large interfacial areas in the PVDF/BT nanocomposites promote the interfacial exchange coupling through a dipolar interface layer, thereby leading to enhanced polarization and K.

In addition to the ferroelectric ceramic nanoparticles, numerous nano-sized oxide particles like MgO, TiO_2, SiO_2, and ZrO_2 have been employed in the development of ferroelectric polymer nanocomposites to obtain enhanced dielectric properties and

capacitive performance. For example, an effective strategy to considerably improve the E_b of the PVDF composites by introducing a small amount (2 wt%) of silane coupling agent (KH550) modified MgO nanoparticles was presented by Chen et al.[80] The Weibull E_b and the maximal energy density have been increased from ~314.5 MV m^{-1} and ~2.03 J cm^{-3} for the pristine PVDF to ~501.4 MV m^{-1} and ~10.52 J cm^{-3} for the PVDF/MgO nanocomposite, respectively, and charge–discharge efficiency is also improved. These results are ascribed to the traps introduced by MgO nanoparticles into polymer matrix, thereby reducing the charge injection and space charge formation. Moreover, a new class of nanocomposites composed of P(VDF-TrFE-CTFE) and TiO_2 nanoparticles that are surface-functionalized by aqueous CO_2-free barium hydroxide were prepared in Wang group.[30] The K of terpolymer (i.e.~42) at 1 kHz is rather close to TiO_2 (~47), which mitigates the formation of unevenly distributed electric fields as a result of the components with markedly different dielectric constants. The enhancements in electric displacement and energy density at high fields are demonstrated in the P(VDF-TrFE-CTFE)/TiO_2 nanocomposites with smaller crystalline domains and higher degree of crystallinities in comparison with the pristine terpolymer. For the nanocomposites with 10 vol% TiO_2, the energy density is ~6.9 J cm^{-3} at 200 MV m^{-1}, which represents a ~45% increase in comparison with the pristine terpolymer with an energy density of ~4.7 J cm^{-3} (**Figure 6**a). It is found that the existence of the interfaces between nanoparticles and polymer matrix in this nanocomposite is evidenced in the temperature dependent spectra of the K (Figure 6b). A shift of the dielectric relaxation peak toward a lower temperature and a reduced loss

tangent are presumably indicative of interface polarization interaction and an increased trap density in the nanocomposites. Following this work, Li et al. functionalized the P(VDF-CTFE)-based copolymers with phosphonic acid terminal groups and subsequently utilized the reactive end-groups of the polymer for direct coupling with ZrO_2 nanoparticles.[78] It is found that covalent assembly of polymer matrix and inorganic filler not only leads to highly dispersed nanoparticles in the matrix but also provides great stability and offers enhanced interfacial interactions for high polarization under the applied electric fields. A greatly enhanced energy density of ~11.2 J cm^{-3} is demonstrated in the nanocomposites of the phosphonic acid-functionalized P(VDF-CTFE) with 9.1 wt% ZrO_2 at 270 MV m^{-1}, which corresponds to a 60% increase in comparison with the pristine copolymer. The improvement in the energy density of the nanocomposites is attributed to the uniform nanoparticle dispersion and the increase of the electric displacement induced by the ZrO_2 nanoparticles. More recently, Dong and coworkers developed a flexible, transparent and high-*K* P(VDF-HFP)-based nanocomposites with fluoride-constructed filler/polymer interfaces.[79] It is found that the composites containing SiO_2 nanoparticles with fluoride-functionalized surface exhibit more induced polar phases, ameliorated interfaces and smaller crystallite sizes, resulting in a high *K* of ~27.1 (at 1 kHz) and a low loss tangent of ~0.03 for the P(VDF-HFP) composite with 20 wt% SiO_2. However, E_b decrease steadily with increasing filler loading. The nanocomposite with 10 wt% SiO_2 exhibits an energy density of ~5.1 J cm^{-3} at the E_b of 390 MV m^{-1}, which is only slightly higher than that of the pristine copolymer (i.e. ~4.8 J cm^{-3} at 410 MV m^{-1}).

Furthermore, Zheng et al. incorporated an organic rubber nanoparticle (methyl methacrylate-butadiene-styrene, MBS) into PVDF matrix to fabricate the PVDF/MBS all-organic nanocomposites with homogeneous dispersions.[119] The nanocomposite with 12 vol% MBS exhibits a maximal energy density of ~9.85 J cm^{-3} at 535 MV m^{-1}, which is ~2.2 times greater than that of pristine PVDF. These improvements in both E_b and energy density are owing to the entanglement between MBS nanoparticles and random chains of polymer, which can reduce the defects and voids in the nanocomposites.

3.1.2. Nanocomposites Based on One-Dimensional Fillers

One-dimensional fillers have a very high aspect ratio and can be overlapped with each other in polymer matrix at a relatively small loading. Among various one-dimensional fillers, ferroelectric ceramic-based nanowires and nanofibers such as BT and BST,[120, 121] are the most frequently studied one-dimensional high-*K* fillers for dielectric polymer composites.

For instance, Tang et al used high aspect ratio BT nanowires with ethylenediamine-modified surface to fabricate the P(VDF-TrFE-CFE)/BT nanocomposites.[120] For the composite with 17.5 vol% BT nanowires, *K* reaches up to ~69.5 at 1 kHz while the loss tangent maintains at a low value of ~0.09. The nanocomposite also shows more than 45.3% increase in energy density, e.g. ~10.48 J cm^{-3} in comparison with ~7.21 J cm^{-3} of the pristine terpolymer at 300 MV m^{-1}. In addition, DOPA was employed in the surface functionalization of BT nanofibers.[92] It is reported by Song et al., the P(VDF-

TrFE) composite with 10.8 vol% DOPA-modified BT nanofibers exhibits an improved K of ~30 at 1 kHz, along with a low loss tangent of ~0.02, and a E_b of ~205 MV m^{-1}. In addition to BT nanofibers and nanowires, Song et al. synthesized DOPA-modified $Ba_{0.6}Sr_{0.4}TiO_3$ nanofibers and incorporated them into PVDF matrix.[122] The E_b of the nanocomposites reaches up to a maximum of ~405.5 MV m^{-1} with 2.1 vol% BST nanofibers and then decreases to ~308.8 MV m^{-1} at the highest BST loading of 11.2 vol%, in comparison with ~380.1 MV m^{-1} of the pristine PVDF. The maximal energy density of ~5.24 J cm^{-3} is achieved with 4.4 vol% BST, which is over two-fold larger than that of the pristine PVDF (i.e. 2.45 J cm^{-3}). The improved E_b and the enhanced energy density is attributed to the combined effects of surface functionalization by dopamine and high aspect ratio of the paraelectric BST nanofibers. Tang et al. studied the PVDF nanocomposites with ethylenediamine-modified $Ba_{0.2}Sr_{0.8}TiO_3$ nanowires.[123] For the nanocomposite with 7.5 vol% BST nanowires, the energy density is ~14.86 J cm^{-3} at 450 MV m^{-1}, which represents a ~42.9% increase in comparison with the pristine PVDF (~10.4 J cm^{-3}) at the same electric field. They also extended their study by employing TiO_2 nanowires as one-dimensional fillers, where APS was used to modify the surface of TiO_2.[91] For the PVDF composite with 7.5 vol% TiO_2 nanowires, K is ~16 at 1 kHz, and the energy density is of ~12.4 J cm^{-3} at the E_b of ~450 MV m^{-1}.

Core-shell structure is also designed for one-dimensional nanofillers to improve the compatibility between nanofillers and polymer matrix to obtain homogeneous nanostructures.[109, 124] PVP has been utilized to prepare the shell structures of $SrTiO_3$

(ST) and $Ba(Zr_{0.3}Ti_{0.7})O_3$ (BZT) nanofibers in Zhai group.[125, 126] The PVDF composites with 2.5 vol% ST@PVP nanofibers and BZT@PVP nanofibers exhibit the energy densities of ~6.8 J cm^{-3} and ~6.3 J cm^{-3} at 380 MV m^{-1}, respectively. Both values are more than two-fold larger than that of the pristine PVDF (i.e. ~2.8 J cm^{-3} at 400 MV m^{-1}). Zhai and coworkers also synthesized a lead-free $0.5(Ba_{0.7}Ca_{0.3})$-TiO_3-$0.5Ba(Zr_{0.2}Ti_{0.8})O_3$ (BCZT) nanofiber via electrospinning (**Figure 7**a), whose surface was then coated using polypropylene acyl tetraethylene pentamine (PATP) as a shell layer (Figure 7b).[127] As shown in Figure 7c, the *K* of both PVDF/BCZT and PVDF/BCZT@PATP nanocomposites increase gradually while the loss tangent decrease with the increase of the filler loading. At the same filler loading, the PVDF/BCZT@PATP nanocomposites exhibit higher *K* and lower loss tangent in comparison with the PVDF/BCZT nanocomposites, which is attributed to the good dispersion and interaction of the fillers via chemical bonding, as well as the confined movement of the charge carriers at the shell layer. The *K* reaches up to ~25.5 at 1 kHz with 9.2 vol% BCZT@PATP nanofibers, which is ~320% times that of the pristine PVDF (i.e. ~8.26). Moreover, the energy density of ~8.23 J cm^{-3} is obtained at 380 MV m^{-1} with a small loading (2.1 vol%) of BCZT@PATP nanofibers. Recently, a bio-inspired approach was reported by Wang et al. They incorporated bio-based fluoro-polydopamine (*f*-DOPA) functionalized BT nanowires into P(VDF-HFP) to form the nanocomposites.[128] The functionalized BT nanowires with a shell layer of *f*-DOPA guarantees the improved compatibility between nanofibers and polymer matrix and the maintenance of E_b, resulting in significantly enhanced energy storage capability. As a

result, the P(VDF-HFP) composite with 5 vol% BT@*f*-DOPA nanowires exhibits an energy density of ~12.87 J cm^{-3} at 480 MV m^{-1}.

Similar to the inorganic-inorganic architecture of shell layer for nanoparticles, inorganic oxide shells have also been designed to surface-functionalize one-dimensional nanofillers.[129] BT@Al_2O_3 nanofibers with a core-shell structure were prepared by Pan et al. via a coaxial electrospinning process. The incorporation of 5 vol% BT@Al_2O_3 nanofibers into PVDF prompts the E_b reaches up to 400 MV m^{-1} and an energy density of ~12.18 J cm^{-3}. Besides, Nan and coworkers designed the structure of BT@TiO_2 nanofibers via a modified electrospinning process, where BT nanoparticles are embedded in TiO_2 nanofiber (**Figure 8**a).[130] A high K of ~41 is obtained from the PVDF/BT@TiO_2 nanocomposite at a volume fraction of ~10%, which is attributed to the percolation of the interfaces between BT and TiO_2, giving rise to the significant enhanced interfacial polarization of the BT@TiO_2 nanofibers in the nanocomposites. More importantly, as seen in Figure 8b, an improved E_b of ~650 MV m^{-1} and an ultrahigh energy density of ~21.2 J cm^{-3} are achieved in the nanocomposite with 3 vol% BT@TiO_2 nanofibers by taking advantage of the high aspect ratio of the nanofibers. Following this work, the P(VDF/HFP)/BT@TiO_2 nanofibers nanocomposites were prepared using P(VDF-HFP) as the polymer matrix owing to its higher K and greater E_b than those of PVDF.[131] A giant energy density of ~31.2 J cm^{-3} at 797.7 MV m^{-1} with a high discharge efficiency of ~78% are achieved in the nanocomposite with 3 vol% BT@TiO_2 nanofibers, which is ~200% enhancement over the pristine P(VDF-HFP) (i.e. ~17.3 J cm^{-3} at 684.3 MV m^{-1}).

3.1.3. Nanocomposites Based on Two-Dimensional Fillers

Recently, two-dimensional fillers with single or only several layers such as BN nanosheets (BNNSs),[37] ZrO_2 nanosheets[132] and kaolinite clay nanosheets (KCNSs)[133] have been employed in the design of ferroelectric polymer nanocomposites with enhanced dielectric properties.

Hexagonal boron nitride (*h*-BN) is a wide band gap (~6 eV) insulator with a E_b around 800 MV m^{-1} and a thermal conductivity as good as graphite.[134, 135] BNNS was selected as the filler to develop the P(VDF-TrFE-CFE)/BNNSs nanocomposites in Wang group.[37] It is observed in **Figure 9**a that the BNNSs are intimately and homogeneously dispersed in the terpolymer matrix owing to the polar surface induced by B-N bonds. The uniform and dense network-like structured nanosheets act as an insulating barrier against leakage current and space charge conduction, and thus help to prevent dielectric failure, resulting in greatly enhanced E_b and less scattering in the experimental data. (Figure 9b). As can be seen in Figure 9c, the energy density of the terpolymer nanocomposite with 12 wt% of BNNSs reaches up to 20.3 J cm^{-3} at 650 MV m^{-1}, which represents a ~121% improvement over the pristine terpolymer measured at 400 MV m^{-1}. The P(VDF-TrFE-CFE)/BNNSs nanocomposite with 12 wt% BNNSs also shows significantly higher charge–discharge efficiencies, e.g., ~83% at 300 MV m^{-1} and ~80% at 600 MV m^{-1}. It should be noted that the thermal conductivity is increased by six times, from ~0.2 W m^{-1} K^{-1} for the pristine terpolymer to over 1.4 W m^{-1} K^{-1} for the nanocomposite with 14 wt% BNNSs, which is of great significance

to benefit stability and lifetime of polymer capacitors. Shen et al. utilized two-dimensional ZrO_2 nanosheets exfoliated from $ZrClO_2 \cdot 8H_2O$ powders to fabricate the PVDF/ZrO_2 nanocomposites.[132] The *K* exhibits a slight drop with increasing ZrO_2 nanosheets content, e.g., the *K* decreases from ~11.2 at 100 Hz for pristine PVDF to ~10.8 for the nanocomposites with 1 wt% ZrO_2. However, an enhanced E_b of 519 MV m^{-1} and a higher energy density of ~11.03 J cm^{-3} is obtained in the PVDF/ZrO_2 (1 wt%) nanocomposite in comparison with pristine PVDF of ~8.18 J cm^{-3} at its E_b of ~416 MV m^{-1}. It is reported by Tomer et al. that 3-merraptnpropylt rimethnxysilane (TTS) was utilized to functionalize KCNSs.[133] The P(VDF-HFP)/TTS-KCNSs nanocomposites are prepared using solution cast method. The incorporation of TTS-KCNSs not only increases the E_b, but also reduces the remnant polarization. The nanocomposite with 5 vol% TTS-KCNSs exhibits a E_b of 780 MV m^{-1} and an enhanced energy density of ~19 J cm^{-3}, which is nearly two-fold larger that of P(VDF-HFP).

In the resulting two-phase ferroelectric polymer nanocomposites, various zero-, one- and two-dimensional nanostructured fillers are used to obtain the increase in interface areas and the enhancement in MWS polarization under the applied fields. The high *K* ceramic fillers such as BT and BST are selected to increase the *K* value and then improve the electric displacement of the nanocomposites. The fillers with relatively low *K* such as SiO_2, ZrO_2 and Al_2O_3 are selected as insulating barriers to reduce leakage current and resist dielectric breakdown in the nanocomposites. Compared with zero-dimensional fillers, one- and two-dimensional fillers have higher aspect ratio and can be overlapped with each other in polymer matrix at a relatively small loading. As a

result, their percolation thresholds are lower and the enhancement in electric displacements are greater than those of the zero-dimensional particles in polymer matrix. Owing to the special lamellar structures, two-dimensional filler like BNNS acts as an insulating barrier against leakage current and space charge conduction, thereby resulting in much reduced remnant polarization and greatly enhanced E_b. In addition, due to the high surface energy of nanofillers as well as the dissimilar physical and chemical surface properties between nanofillers and polymer matrixes, surface modification agents with functionalized groups, such as silane, dopamine and phosphonic acid are successfully employed in the nanocomposite strategies to improve the compatibility of filler/polymer interfaces and reduce the agglomeration of fillers in composites. The design of core-shell structure is also considered as an effective functionalization approach for fillers to enhance the energy storage capacity of nanocomposites. Organic shells like PVP and PMMA help to improve the interface compatibility between filler and polymer matrix, thus obtaining the composites with homogeneous nanostructures. Inorganic shells such as Al_2O_3 and TiO_2 with relatively low *K*, also been utilized as a buffer between high *K* ceramic fillers and ferroelectric polymer matrixes, which help to alleviate local field distortion in the composites resulting from a large mismatch in *K* values between fillers and polymers

3.2. Ferroelectric Nanocomposites Based on Heterogeneous Composition

In this section, the heterogeneous composition refers to the inclusion of two or more fillers in the nanocomposites. This approach has a great potential in combining the

distinct advantages of each component to improve the overall dielectric properties and capacitive performance of the resulting composites.[136–138]

Yu et al. designed a class of ternary nanocomposites via incorporating a third component (polyacrylate elastomer (AR71)) into a PVDF/BT composition system.[139] The incorporated AR71 particles have little effect on the *K* of the PVDF/BT nanocomposites. However, a small amount of space charges are induced by the AR71 particles, resulting in the enhanced MWS interfacial polarization, space charge polarization and the improved electric displacement of the nanocomposites. Moreover, the AR71 particles can produce large elastic deformation under the applied electric field, which increases the accumulation and the polarization of space charge, indirectly increasing the energy density. The multi-phased nanocomposite with 5 vol% BT and 3 vol% AR71 exhibits a maximal energy density of ~8.8 J /cm^3 at 400 MV m^{-1}. In Jang group, graphene nanodots (GNDs) were synthesized via excessive chemical oxidation of carbon nanofibers (CNFs), followed by amination using ethylenediamine (EDA) to obtain the amino-functionalized graphene nanodots (NH_2-treated GNDs).[140] The ternary PVDF/NH_2-treated GNDs/reduced graphene oxide (RGO) nanocomposites are fabricated via the inclusion of two kinds of nanofiller into PVDF matrix. The incorporation of the NH_2-GNDs improves the dispersibility and compatibility of the two-dimensional RGO filler in polymer. The ternary nanocomposite with 10 vol% nanofillers exhibits a high *K* of ~60.6 at 1 kHz, an E_b of ~390 MV m^{-1}, and an energy density of ~14.1 J cm^{-3}. These results are credited to the synergistic effect of NH_2-GNDs and RGO which inhibits the movement of PVDF molecular chains, thereby

reducing the relaxation loss and dipole rotation loss. Interestingly, an effective ternary-composite approach to increase the K using BT nanoparticles as well as to improve E_b using BNNSs were brought out by Li et al.[24] It is found that the incorporation of BNNSs improves the dispersibility of BT nanoparticles in the polymer matrix, thus the P(VDF-CTFE)/BT/BNNSs nanocomposites with homogeneous nanostructures are obtained as shown in **Figure 10**a and 10b. The highest energy density of ~21.2 J cm^{-3} along with a high charge–discharge efficiency of ~78% are obtained from the ternary polymer nanocomposites with 12 wt% BNNSs and 15 wt% BT nanoparticles. The ternary composite has a K of ~12 and an E_b of ~552 MV m^{-1}, representing a ~20% increase in K along with a ~43% improvement in E_b in comparison with the pristine copolymer. Recently, Jin et al. reported an organic-inorganic hybrid nanocomposite composed of both silane-functionalized BT nanoparticles and multi-walled carbon nanotubes (MWCNTs) embedded in the ferroelectric polymer.[141] A nice combination of K of ~71.7 and a loss tangent of ~0.045 are obtained from the P(VDF-HFP) nanocomposite containing 37.1 vol% BT and 3 vol% MWCNTs. The calculated energy density of this nanocomposite is ~19.82 J cm^{-3} at 250 MV m^{-1}.

To sum up, the incorporation of multiple nanofillers with complementary functionalities into ferroelectric polymers combines the distinct advantages of each component to enhance the capacitive energy storage performance of the resulting composites. Interestingly, the incorporation of the third component improves the dispersibility of nano-sized fillers in ternary composites with much homogeneous nanostructures. However, there is a striking lack of fundamental understanding of the

synergistic effects of the multiple components in the composites and the dielectric failure mechanisms in heterogeneous compositions under the applied electric fields.

3.3. Ferroelectric Nanocomposites Based on Hierarchical Structures

Hierarchical structures, including alignment of fillers in polymer matrix[142, 143] and multi-layered structure of composites[25, 144] et al., have been developed for ferroelectric polymer nanocomposites to obtain enhanced dielectric constant, low loss, improved E_b, and high energy density.

3.3.1. Nanocomposites Based on Alignment of Fillers

The anisotropy in dielectrics is useful to control the properties in different dimensions.[145] For polymer nanocomposites, the dielectric anisotropy can be achieved via 1) incorporating one-dimensional or two-dimensional anisotropic nanofillers with high aspect ratios into polymer matrix through external assistance, e.g., mechanical stretching and electric field induction,[146] 2) attaching zero-dimensional nanoparticles onto the skeleton with a hierarchical structure, e.g., three-dimensional cellulose skeletons.[142]

A simple strategy for aligning nanowires in PVDF was presented by Tang et al.[147] The PVDF nanocomposites with aligned $PbZr_{0.2}Ti_{0.8}O_3$ (PZT) nanowires are prepared by a uniaxial strain assembly method. It is found that the K of 3-direction aligned nanocomposites is much larger than that of the PVDF composites with random PZT at the same loading, e.g., ~34 of the aligned nanocomposite vs. ~25 of the random nanocomposite at 30 vol% PZT. In addition, the composite with 40 vol% aligned PZT

in PVDF can achieve a maximal calculated energy density of ~1.28 J cm^{-3} at a low electric field of 15 MV m^{-1}. Recently, Xie et al developed a physical-assisted casting method for the alignment of 3 vol% elongated BT nanowires in P(VDF-CTFE) to form the P(VDF-CTFE)/BT Z-aligned and X–Y-aligned nanocomposites (**Figure 11**a and 11b).[148] It is found that both *K* and electric conductivity of the Z-aligned nanocomposites are higher than those of the X–Y-aligned nanocomposites, which is attributed to the enhanced electric polarization along the Z-aligned directions in the nanocomposites. As can be seen in Figure 11c, the X–Y-aligned nanocomposite exhibits the maximal energy density of ~10.1 J cm^{-3} and an efficiency of ~56.8% at the E_b of 340 MV m^{-1}. However, the Z-aligned nanocomposite exhibits a higher maximal energy density of ~10.8 J cm^{-3} and a better efficiency of ~61.4% at an electric field of 240 MV m^{-1}. In Zhai group, they synthesized a highly oriented one-dimensional TiO_2 nanorod array via hydrothermal reaction method and then prepared the polymer nanocomposites by embedding PVDF into the nanorod interspace and onto the nanorod surface using spin-coating method.[149] For the PVDF nanocomposite with the rod-shaped array length of ~1.8 μm and a film thickness of ~10 μm, the maximal energy density of 10.62 J cm^{-3} is obtained at 340 MV m^{-1} with an efficiency of ~70%. This density is around 3.5 times higher than that of the pristine PVDF at the same electric field. A highly-oriented one-dimensional BT nanorod array was reported in their following work,[150] in which a higher energy density of 11.82 J cm^{-3} at 320 MV m^{-1} is achieved in the PVDF/BT nanorod arrayed nanocomposite.

3.3.2. Nanocomposites Based on Multi-Layered Structures

More recently, it is found that the multi-layer structured polymer composites can not only adjust the electric field distribution in composite films at a macroscopic level but also combine the advantage of each layer to achieve a simultaneous enhancement in both E_b and energy density.[151–155]

Nan and coworkers reported a three-layer sandwich-structured nanocomposite consisting of a central layer from the PVDF/BT nanofibers composites and two outer layers from the PVDF/BT nanoparticles composites.[156] The outer layers with high volume fraction BT nanoparticles are designed to induce high electric polarization, while the central layer with oriented BT nanofibers exhibits lower K and can withstand much higher electric fields. The maximal K of ~25 with a low loss tangent of ~0.04 is achieved in the sandwich-structured PVDF composite film containing 3 vol% BT nanofibers in the central layer and 30 vol% BT nanoparticles in the outer layers. An energy density of ~9.72 J cm^{-3} at 453 MV m^{-1} is obtained at the loading of 2 vol% BT nanofibers in the central layer and 10 vol% BT nanoparticles in the outer layers. Following this work, they designed sandwich-structured nanocomposite films with two reversed topological configurations structures (BGB and GBG) via hot-pressing method (**Figure 12**).[157] The nanocomposites are made from two different layers, e.g., PVDF/GO-TiO_2 (G-layers) and PVDF/BST (B-layers) using either graphene oxide nanosheets coated with TiO_2 (GO-TiO_2) or $Ba_{0.6}Sr_{0.4}TiO_3$ nanofibers. Benefiting from the enhancement in both electric polarization and E_b, an energy density of ~14.6 J cm^{-3} at 450 MV m^{-1} is achieved in the BGB nanocomposite containing 10 wt% GO-TiO_2 in the central layer and 3 vol% BST nanofibers in the outer layers. Wang et al. also

cleverly designed the sandwich-structured films containing a hard layer and two soft layers seen in **Figure 13**a and 13b.[158] In this structure, the central layer with small amount (only 1 vol%) of BT nanoparticles and the outer layers with various volume fractions (10–50 vol%) of BT nanoparticles are considered as hard layer and soft layers, respectively. The *K* increases with increasing filler loading in the soft layers, achieving the maximal value of ~35 at 1 kHz. The hard layer is designed to limit the electron tunneling through the filler/matrix interfaces and block the growth of electrical trees before dielectric breakdown while the soft layers are to induce the high electric polarization and achieve higher *K*, resulting in an enhanced E_b of ~470 MV m^{-1} along with a high energy density of ~18.8 J cm^{-3} with the BT volume fractions of 1 vol% in hard layer and 20 vol% in soft layers. Following this work, the PVDF-based sandwich-structured films were fabricated via incorporating DOPA-functionalized BT nanoparticles.[159] It is found that an energy density of ~16.8 J cm^{-3} along with a high charge–discharge efficiency of ~70% are achieved in the sandwich-structured film with pristine PVDF as the central layer and the PVDF composite with 3 vol% BT nanoparticles as the outer layers. Furthermore, a class of gradient-layered nanocomposites (GLN) were reported in their following work.[160] The filler loading of BT nanoparticles gradually increases from the upper layer to the bottom layer to form two gradient boundaries in the PVDF-based GLN films. Distinctively different from the sandwich-structured composites described above, in which the outer layers are in the same composition, GLN presents an approach towards dielectrics with highly enhanced E_b by constructing a gradient electric field distribution. Consequently,

gradually increased loadings of BT filler are introduced into the middle and bottom layers of the GLN to enlarge the difference of electric field in each layer, which can simultaneously improve the resistance of the growth of electrical tree and enhance electric displacement. As a result, an E_b of ~390 MV m^{-1} along with an energy density of ~16.5 J cm^{-3} are obtained in the gradient-layered film with 1 vol% BT in the upper layer, 10 vol% BT in the middle layer and 20 vol% BT in the bottom layer.

Different from those previous sandwich-structured films containing ferroelectric ceramic fillers in the outer layers, Liu et al. designed a class of the sandwich-structured nanocomposite composed of an outer layer with the incorporation of highly insulating fillers BNNSs into PVDF matrix to achieve a significantly improved E_b, whereas the central layer is filled with the high K fillers $Ba_{0.5}Sr_{0.5}TiO_3$ nanowires to induce high electric polarization as seen in **Figure 13**c and 13d.[161] By varying BST concentration in the central layer, the electrical trees can be blocked inside the central layer. The Weibull E_b increases to the maximized value of 588 MV m^{-1} and then decreases with further increase of BST content. A high energy density of 20.5 J cm^{-3} at its Weibull E_b is obtained from the sandwich-structured PVDF composite film containing 8 vol% BST nanowires in the central layer and 10 vol% BNNSs in the outer layers. Recently, the PVDF/two-dimensional platelets nanocomposites with a sandwich-structure have been reported by Pan et al..[162] The sandwich-structured nanocomposite film fabricated from pristine PVDF as the central layer and the PVDF composite with 5 vol% $NaNbO_3$ nanoplatelets as the outer layers exhibits a maximal energy density of ~13.5 J cm^{-3} at 400 MV m^{-1}.

The resulting ferroelectric polymer nanocomposites based on hierarchical structures integrate unique properties arisen from rationally-designed structural organization for the improvement of capacitive energy storage. With the spatial arrangement of inorganic fillers in nanostructured composites, an increase of K can be obtained by the enhanced electric polarization along the direction of the aligned nanofillers. Accordingly, an improvement of E_b is owing to the incorporated one- or two-dimensional nanofillers that are perpendicular to the direction of the external electric field, which can effectively mitigate the distortion of local field. In addition, the approach of layer-structured ferroelectric polymer nanocomposites can not only adjust the electric field distribution in the composite films at a macroscopic level but also combine the advantages of each layer. For example, the layer filled with high content of ceramic fillers are designed to induce high electric polarization and achieve higher K, while the other layer can block electrical trees growth and withstand higher electric fields before breakdown. This is considered as a very promising approach to high-performance dielectric materials with much reduced loss and a simultaneous large improvement in both E_b and energy density.

4. Summary and Perspective

The field of ferroelectric polymer nanocomposite-based dielectric materials has witnessed much exciting progress over the past several years, and the pace of progress has continued to accelerate. By utilizing the intrinsic advantages of ferroelectric polymers such as the highest dielectric constant among the known polymers, the energy

densities of ferroelectric polymer nanocomposites have been improved significantly to become the state-of-the-art values, e.g. > 20 J cm^{-3}. The improvement of energy density of polymer dielectrics represents a key element in meeting the technological challenges and fulfilling the miniaturization requirements of advanced electronics and electrical power systems. The field of ferroelectric polymer-based dielectric materials has been plagued by a well-known paradox, which is inherently high loss associated with ferroelectric polymers. The enhancement of dielectric constant in many cases might not lead to actual improvement of discharged energy density owing to exponentially increased dielectric loss and associated degraded charge–discharge efficiency with electric field. Various innovative approaches, including surface-functionalized fillers, introduction of wide-band-gap fillers, and cross-linking, have been designed to efficiently suppress the dielectric loss, especially high-field loss, of ferroelectric polymer composites while taking advantage of their high dielectric constants. As a result, the discharged energy densities of the ferroelectric polymer composites have outperformed all the other polymer dielectrics. In particular, the spatial arrangement of inorganic fillers with complementary functionalities into layered ferroelectric polymers developed from Nan and Wang groups has been demonstrated to be a very efficient approach to high-performance dielectric materials with greatly improved energy density and much reduced loss.[156–161]

However, the challenges we are facing are also overwhelming as several crucial issues remain to be addressed. The charge–discharge efficiency of the ferroelectric polymer composites needs to be increased significantly in order to reach the level

comparable to BOPP for practical capacitor applications. In addition to conduction loss that is common to all the dielectric materials, polarization hysteresis is a loss mechanism uniquely belonging to ferroelectric materials. Molecular structures of ferroelectric polymers have to be further optimized to reduce the hysteresis loss. The polarization coupling at the filler/polymer interfaces must be utilized to enhance capacitive performance at high electric fields. There is a striking lack of fundamental understanding of the interfacial coupling of the electroactive components in the composites and the correction between ferroelectric polymer compositions and their dielectric properties under the applied electric fields. Theoretical simulations at multiple length scales are important for us to understand the polarization, electric field distribution, and breakdown mechanisms of the ferroelectric polymer nanocomposites.[157–164] The critical issues related to mass fabrication of dielectric polymer nanocomposite thin films are yet to addressed. While the majority of the composite films are solution-processed in laboratory settings, conventional polymer dielectric films are actually produced via melt processes. The possibility of producing the composite thin films with thickness ≤10 μm in a manufacturing setting needs to be tackled. Truly low-cost manufacturable methods for fabrication of ferroelectric polymer composite thin films and prototype capacitors need to be demonstrated. As a highly interdisciplinary field, progress in the ferroelectric polymer composite based dielectrics is critically dependent on successful interactions across the boundaries of traditional disciplines. Rapid advances are to be anticipated through collaborative efforts from synthetic chemists, materials scientists and engineers, and electrical engineers.

Acknowledgements

The work at The Pennsylvania State University was supported by the U.S. Office of Naval Research. H.L. acknowledges the financial support from the China Scholarship Council (CSC).

Received: ((will be filled in by the editorial staff))
Revised: ((will be filled in by the editorial staff))
Published online: ((will be filled in by the editorial staff))

References

[1] M. S. Whittingham, *MRS Bull.* **2008**, *33*, 411.
[2] Q. Wang, L. Zhu, *J. Polym. Sci., Part B: Polym. Phys.* **2011**, *49*, 1421.
[3] N. S. Hasan, M. Y. Hassan, M. S. Majid, H. A. Rahman, *Renew. Sust. Energ. Rev.* **2013**, *21*, 237.
[4] R. M. Dell, D. A. Rand, *J. Power Sources* **2001**, *100*, 2.
[5] T. Kousksou, P. Bruel, A. Jamil, T. El Rhafiki, Y. Zeraouli, *Sol. Energ. Mat. Sol. C* **2014**, *120*, 59.
[6] A. S. Aricò, P. Bruce, B. Scrosati, J.-M. Tarascon, W. Van Schalkwijk, *Nat. Mater.* **2005**, *4*, 366.
[7] X. Luo, J. Wang, M. Dooner, J. Clarke, *Appl. Energy* **2015**, *137*, 511.
[8] B. Dunn, H. Kamath, J. M. Tarascon, *Science* **2011**, *334*, 928.
[9] P. Simon, Y. Gogotsi, B. Dunn, *Science* **2014**, *343*, 1210.
[10] Y. Wang, Y. Xia, *Adv. Mater.* **2013**, *25*, 5336.
[11] G. Qu, J. Cheng, X. Li, D. Yuan, P. Chen, X. Chen, B. Wang, H. Peng, *Adv. Mater.* **2016**, *28*, 3646.
[12] J. Ren, L. Li, C. Chen, X. Chen, Z. Cai, L. Qiu, Y. Wang, X. Zhu, H. Peng, *Adv. Mater.* **2013**, *25*, 1155.
[13] Z. Yang, J. Ren, Z. Zhang, X. Chen, G. Guan, L. Qiu, Y. Zhang, H. Peng, *Chem. Rev.* **2015**, *115*, 5159.
[14] J. Pan, K. Li, S. Chuayprakong, T. Hsu, Q. Wang, *ACS Appl. Mater. Interfaces* **2010**, *2*, 1286.
[15] Z. M. Dang, J. K. Yuan, S. H. Yao, R. J. Liao, *Adv. Mater.* **2013**, *25*, 6334.
[16] Q. Li, Q. Wang, *Macromol. Chem. Phys.* **2016**, *217*, 1228.
[17] Y. Cao, P. C. Irwin, K. Younsi, *IEEE Trans. Dielectr. Electr. Insul.* **2004**, *11*, 797.
[18] V. K. Thakur, R. K. Gupta, *Chem. Rev.* **2016**, *116*, 4260.
[19] M. Rabuffi, G. Picci, *IEEE Trans. Plasma Sci.* **2002**, *30*, 1939.
[20] X. Hao, *J. Adv. Dielectr.* **2013**, *3*, 1330001.

[21] Q. Chen, Y. Shen, S. Zhang, Q. M. Zhang, *Annu. Rev. Mater. Res.* **2015**, *45*, 433.
[22] Y. Shen, Y. Lin, Q. M. Zhang, *MRS Bull.* **2015**, *40*, 753.
[23] B. Chu, X. Zhou, K. Ren, B. Neese, M. Lin, Q. Wang, F. Bauer, Q. M. Zhang, *Science* **2006**, *313*, 334.
[24] Q. Li, K. Han, M. R. Gadinski, G. Zhang, Q. Wang, *Adv. Mater.* **2014**, *26*, 6244.
[25] Q. Li, F. Liu, T. Yang, M. R. Gadinski, G. Zhang, L.-Q. Chen, Q. Wang, *Proc. Natl. Acad. Sci. U. S. A.* **2016**, *113*, 9995.
[26] J. R. Laghari, W. J. Sarjeant, *IEEE Trans. Power Electr.* **1992**, *7*, 251.
[27] Z. Yao, Z. Song, H. Hao, Z. Yu, M. Cao, S. Zhang, M. T. Lanagan, H. Liu, *Adv. Mater.* **2017**, *29*, 1601727.
[28] W. J. Sarjeant, J. Zirnheld, F. W. MacDougall, *IEEE Trans. Plasma Sci.* **1998**, *26*, 1368.
[29] W. Sarjeant, I. W. Clelland, R. A. Price, *Proc. IEEE* **2001**, *89*, 846.
[30] J. Li, S. I. Seok, B. Chu, F. Dogan, Q. M. Zhang, Q. Wang, *Adv. Mater.* **2009**, *21*, 217.
[31] M. Roy, J. Nelson, R. MacCrone, L. S. Schadler, C. Reed, R. Keefe, *IEEE Trans. Dielectr. Electr. Insul.* **2005**, *12*, 629.
[32] T. Tanaka, M. Kozako, N. Fuse, Y. Ohki, *IEEE Trans. Dielectr. Electr. Insul.* **2005**, *12*, 669.
[33] K. Yao, S. Chen, M. Rahimabady, M. S. Mirshekarloo, S. Yu, F. H. Tay, T. Sritharan, L. Lu, *IEEE Trans. Ultrason. Ferroelectr. Freq. Control.* **2011**, *58*, 1968.
[34] L. Zhu, Q. Wang, *Macromolecules* **2012**, *45*, 2937.
[35] M. Sebastian, H. Jantunen, *Int. Mater. Rev.* **2008**, *53*, 57.
[36] Q. Li, L. Chen, M. R. Gadinski, S. Zhang, G. Zhang, H. U. Li, E. Iagodkine, A. Haque, L.-Q. Chen, T. N. Jackson, *Nature* **2015**, *523*, 576.
[37] Q. Li, G. Zhang, F. Liu, K. Han, M. R. Gadinski, C. Xiong, Q. Wang, *Energ. Environ. Sci.* **2015**, *8*, 922.
[38] B. Ameduri, *Chem. Rev* **2009**, *109*, 6632.
[39] P. Martins, A. Lopes, S. Lanceros-Mendez, *Prog. Polym. Sci.* **2014**, 39, 683.
[40] W. Li, Q. Meng, Y. Zheng, Z. Zhang, W. Xia, *Appl. Phys. Lett.* **2010**, *96*, 192905.
[41] M. Bachmann, J. Lando, *Macromolecules* **1981**, *14*, 40.
[42] P. Martins, J. S. Nunes, G. Hungerford, D. Miranda, A. Ferreira, V. Sencadas, S. Lanceros-Méndez, *Phys. Lett. A* **2009**, *373*, 177.
[43] F. Guan, J. Wang, J. Pan, Q. Wang, L. Zhu, *Macromolecules* **2010**, *43*, 6739.
[44] D. R. Dillon, K. K. Tenneti, C. Y. Li, F. K. Ko, I. Sics, B. S. Hsiao, *Polymer* **2006**, *47*, 1678.
[45] Q. M. Zhang, V. Bharti, X. Zhao, *Science* **1998**, *280*, 2101.
[46] X. Zhou, B. Chu, B. Neese, M. Lin, Q. M. Zhang, *IEEE Trans. Dielectr. Electr. Insul.* **2007**, *14*, 1133.

[47] Y. Tajitsu, A. Chiba, T. Furukawa, M. Date, E. Fukada, *Appl. Phys. Lett.* **1980**, *36*, 286.
[48] T. Furukawa, *Adv. Colloid Interfac.* **1997**, *71*, 183.
[49] F. Macchi, B. Daudin, J. Legrand, *Ferroelectr.* **1990**, *109*, 303.
[50] X.-Z. Zhao, V. Bharti, Q. Zhang, T. Romotowski, F. Tito, R. Ting, *Appl. Phys. Lett.* **1998**, *73*, 2054.
[51] Z.-Y. Cheng, V. Bharti, T.-B. Xu, H. Xu, T. Mai, Q. M. Zhang, *Sensor Actuat. A - Phys.* **2001**, *90*, 138.
[52] V. Bharti, X.-Z. Zhao, Q. M. Zhang, T. Romotowski, F. Tito, R. Ting, *Mater. Res. Innovations* **1998**, *2*, 57.
[53] J. Forsythe, D. Hill, *Prog. Polym. Sci.* **2000**, *25*, 101.
[54] Z.-Y. Cheng, Q. Zhang, F. B. Bateman, *J. Appl. Phys.* **2002**, *92*, 6749.
[55] Z.-Y. Cheng, D. Olson, H. Xu, F. Xia, J. Hundal, Q. Zhang, F. B. Bateman, G. Kavarnos, T. Ramotowski, *Macromolecules* **2002**, *35*, 664.
[56] P. Khanchaitit, K. Han, M. R. Gadinski, Q. Li, Q. Wang, *Nat. Commun,* **2013**, *4*, 2845.
[57] K. Han, Q. Li, C. Chanthad, M. R. Gadinski, G. Zhang, Q. Wang, *Adv. Funct. Mater.* **2015**, *25*, 3505.
[58] X. Z. Chen, Z. W. Li, Z. X. Cheng, J. Z. Zhang, Q. D. Shen, H. X. Ge, H. T. Li, *Macromol. Rapid Commun.* **2011**, *32*, 94.
[59] F. Guan, J. Pan, J. Wang, Q. Wang, L. Zhu, *Macromolecules* **2009**, *43*, 384.
[60] X. Zhou, X. Zhao, Z. Suo, C. Zou, J. Runt, S. Liu, S. Zhang, Q. M. Zhang, *Appl. Phys. Lett.* **2009**, *94*, 162901.
[61] R. Sousa, J. Nunes-Pereira, J. Ferreira, C. Costa, A. Machado, M. Silva, S. Lanceros-Mendez, *Polym. Test.* **2014**, *40*, 245.
[62] M. R. Gadinski, K. Han, Q. Li, G. Zhang, W. Reainthippayasakul, Q. Wang, *ACS Appl. Mater. Interfaces* **2014**, *6*, 18981.
[63] F. Xia, Z. Y. Cheng, H. Xu, H. Li, Q. Zhang, G. J. Kavarnos, R. Y. Ting, G. Abdul-Sadek, K. D. Belfield, *Adv. Mater.* **2002**, *14*, 1574.
[64] H. Xu, Z.-Y. Cheng, D. Olson, T. Mai, Q. Zhang, G. Kavarnos, *Appl. Phys. Lett.* **2001**, *78*, 2360.
[65] T. Chung, A. Petchsuk, *Macromolecules* **2002**, *35*, 7678.
[66] V. Bobnar, B. Vodopivec, A. Levstik, M. Kosec, B. Hilczer, Q. M. Zhang, *Macromolecules* **2003**, *36*, 4436.
[67] Q. Chen, K. Ren, B. Chu, Y. Liu, Q. M. Zhang, V. Bobnar, A. Levstik, *Ferroelectr.* **2007**, *354*, 178.
[68] C. Ang, Z. Yu, *Adv. Mater.* **2004**, *16*, 979.
[69] Y. Lu, J. Claude, Q. M. Zhang, Q. Wang, *Macromolecules* **2006**, *39*, 6962.
[70] Y. Lu, J. Claude, B. Neese, Q. M. Zhang, Q. Wang, *J. Am. Chem. Soc.* **2006**, *128*, 8120.
[71] Y. Lu, J. Claude, L. E. Norena-Franco, Q. Wang, *J. Phys. Chem. B* **2008**, *112*, 10411.
[72] T. Soulestin, V. Ladmiral, T. Lannuzel, F. Domingues Dos Santos, B. Ameduri, *Macromolecules* **2015**, *48*, 7861.

[73] Z. Zhang, T. M. Chung, *Macromolecules* **2007**, *40*, 783.
[74] M. R. Gadinski, Q. Li, G. Zhang, X. Zhang, Q. Wang, *Macromolecules* **2015**, *48*, 2731.
[75] B. Chu, X. Zhou, B. Neese, Q. M. Zhang, F. Bauer, *IEEE Trans. Dielectr. Electr. Insul.* **2006**, *13*, 1162.
[76] Y. Mao, S. Mao, Z.-G. Ye, Z. Xie, L. Zheng, *J. Appl. Phys.* **2010**, *108*, 014102.
[77] H. Li, C. Wang, Y. Zhang, Z. Guo, H. Wang, Z. Peng, *IEEE Conf. High Volt. Eng. Appl. (ICHVE)* **2016**.
[78] J. Li, P. Khanchaitit, K. Han, Q. Wang, *Chem. Mater.* **2010**, *22*, 5350.
[79] L. Li, R. Feng, Y. Zhang, L. Dong, *J. Mater. Chem. C* **2017**, *5*, 11403.
[80] S. S. Chen, J. Hu, L. Gao, Y. Zhou, S. M. Peng, J. L. He, Z. M. Dang, *RSC Adv.* **2016**, *6*, 33599.
[81] Y. Thakur, M. H. Lean, Q. M. Zhang, *Appl. Phys. Lett.* **2017**, *110*, 122905.
[82] Y. Thakur, T. Zhang, C. Iacob, T. Yang, J. Bernholc, L. Chen, J. Runt, Q. M. Zhang, *Nanoscale* **2017**, *9*, 10992.
[83] B.-H. Fan, J.-W. Zha, D. Wang, J. Zhao, Z.-M. Dang, *Appl. Phys. Lett.* **2012**, *100*, 012903.
[84] T. Zhou, J.-W. Zha, R.-Y. Cui, B.-H. Fan, J.-K. Yuan, Z.-M. Dang, *ACS Appl. Mater. Interfaces* **2011**, *3*, 2184.
[85] W. Xia, Z. Xu, F. Wen, Z. Zhang, *Ceram. Int.* **2012**, *38*, 1071.
[86] K. Li, H. Wang, F. Xiang, W. Liu, H. Yang, *Appl. Phys. Lett.* **2009**, *95*, 202904.
[87] C. Wu, X. Huang, X. Wu, L. Xie, K. Yang, P. Jiang, *Nanoscale* **2013**, *5*, 3847.
[88] Z.-M. Dang, J.-K. Yuan, J.-W. Zha, T. Zhou, S.-T. Li, G.-H. Hu, *Prog. Mater. Sci.* **2012**, *57*, 660.
[89] X. Huang, C. Zhi, P. Jiang, D. Golberg, Y. Bando, T. Tanaka, *Adv. Funct. Mater.* **2013**, *23*, 1824.
[90] S. Liu, J. Zhai, J. Wang, S. Xue, W. Zhang, *ACS Appl. Mater. Interfaces* **2014**, *6*, 1533.
[91] H. Tang, H. A. Sodano, *Appl. Phys. Lett.* **2013**, *102*, 063901.
[92] Y. Song, Y. Shen, H. Liu, Y. Lin, M. Li, C.-W. Nan, *J. Mater. Chem.* **2012**, *22*, 8063.
[93] K. Han, Q. Li, Z. Chen, M. R. Gadinski, L. Dong, C. Xiong, Q. Wang, *J. Mater. Chem. C* **2013**, *1*, 7034.
[94] Q. Jia, X. Huang, G. Wang, J. Diao, P. Jiang, *J. Phys. Chem, C* **2016**, *120*, 10206.
[95] S. K. Ghosh, W. Rahman, T. R. Middya, S. Sen, D. Mandal, *Nanotechnol.* **2016**, *27*, 215401.
[96] S. P. Fillery, H. Koerner, L. Drummy, E. Dunkerley, M. F. Durstock, D. F. Schmidt, R. A. Vaia, *ACS Appl. Mater. Interfaces* **2012**, *4*, 1388.
[97] L. Xing, Q. Li, G. Zhang, X. Zhang, F. Liu, L. Liu, Y. Huang, Q. Wang, *Adv. Funct. Mater.* **2016**, *26*, 3524.

[98] F. Liu, Q. Li, Z. Li, Y. Liu, L. Dong, C. Xiong, Q. Wang, *Compos. Sci. Technol.* **2017**, *142*, 139.
[99] H. Li, C. Wang, Z. Guo, H. Wang, Y. Zhang, R. Hong, Z. Peng, *IEEE Conf. Dielectr. (ICD)* **2016**, *2*, 1036.
[100] Z.-M. Dang, H.-Y. Wang, H.-P. Xu, *Appl. Phys. Lett.* **2006**, *89*, 112902.
[101] K. Yu, H. Wang, Y. Zhou, Y. Bai, Y. Niu, *J. Appl. Phys.* **2013**, *113*, 034105.
[102] J. Li, J. Claude, L. E. Norena-Franco, S. I. Seok, Q. Wang, *Chem. Mater.* **2008**, *20*, 6304.
[103] C. Xu, K. Xu, H. Gu, R. Zheng, H. Liu, X. Zhang, Z. Guo, B. Xu, *J. Am. Chem. Soc.* **2004**, *126*, 9938.
[104] W. Huang, P. Jiang, C. Wei, D. Zhuang, J. Shi, *J. Mater. Res.* **2008**, *23*, 1946.
[105] Y. Song, Y. Shen, H. Liu, Y. Lin, M. Li, C.-W. Nan, *J. Mater. Chem.* **2012**, *22*, 16491.
[106] M.-F. Lin, V. K. Thakur, E. J. Tan, P. S. Lee, *RSC Adv.* **2011**, *1*, 576.
[107] P. Kim, S. C. Jones, P. J. Hotchkiss, J. N. Haddock, B. Kippelen, S. R. Marder, J. W. Perry, *Adv. Mater.* **2007**, *19*, 1001.
[108] P. Kim, N. M. Doss, J. P. Tillotson, P. J. Hotchkiss, M.-J. Pan, S. R. Marder, J. Li, J. P. Calame, J. W. Perry, *ACS Nano* **2009**, *3*, 2581.
[109] X. Huang, P. Jiang, *Adv. Mater.* **2015**, *27*, 546.
[110] Z. Pan, L. Yao, J. Zhai, D. Fu, B. Shen, H. Wang, *ACS Appl. Mater. Interfaces* **2017**, *9*, 4024.
[111] K. Yu, Y. Niu, Y. Zhou, Y. Bai, H. Wang, *J. Am. Ceram. Soc.* **2013**, *96*, 2519.
[112] K. Yang, X. Huang, Y. Huang, L. Xie, P. Jiang, *Chem. Mater.* **2013**, *25*, 2327.
[113] M. Zhu, X. Huang, K. Yang, X. Zhai, J. Zhang, J. He, P. Jiang, *ACS Appl. Mater. Interfaces* **2014**, *6*, 19644.
[114] K. Yu, Y. Niu, Y. Bai, Y. Zhou, H. Wang, *Appl. Phys. Lett.* **2013**, *102*, 102903.
[115] M. Rahimabady, M. S. Mirshekarloo, K. Yao, L. Lu, *Phys. Chem. Chem. Phys.* **2013**, *15*, 16242.
[116] Z. Pan, L. Yao, J. Zhai, B. Shen, S. Liu, H. Wang, J. Liu, *J. Mater. Chem. A* **2016**, *4*, 13259.
[117] K. Yang, X. Huang, J. He, P. Jiang, *Adv. Mater. Interfaces* **2015**, *2*, 1500361.
[118] B. Jiang, X. Pang, B. Li, Z. Lin, *J. Am. Chem. Soc.* **2015**, *137*, 11760.
[119] M.-S. Zheng, J.-W. Zha, Y. Yang, P. Han, C.-H. Hu, Z.-M. Dang, *Appl. Phys. Lett.* **2016**, *109*, 072902.
[120] H. Tang, Y. Lin, H. A. Sodano, *Adv. Energy Mater.* **2013**, *3*, 451.
[121] S. Liu, J. Zhai, *RSC Adv.* **2014**, *4*, 40973.
[122] Y. Song, Y. Shen, P. Hu, Y. Lin, M. Li, C. Nan, *Appl. Phys. Lett.* **2012**, *101*, 152904.
[123] H. Tang, H. A. Sodano, *Nano Lett.* **2013**, *13*, 1373.
[124] G. Wang, X. Huang, P. Jiang, *J. Mater. Chem. C* **2017**, *5*, 3112.
[125] S. Liu, J. Zhai, *J. Mater. Chem. A* **2015**, *3*, 1511.
[126] S. Liu, S. Xue, S. Xiu, B. Shen, J. Zhai, *Sci. Rep.* **2016**, *6*, 26198.

[127] Z. Pan, L. Yao, J. Zhai, H. Wang, B. Shen, *ACS Appl. Mater. Interfaces* **2017**, *9*, 14337.
[128] G. Wang, X. Huang, P. Jiang, *ACS Appl. Mater. Interfaces* **2017**, *9*, 7547.
[129] S. Liu, S. Xue, B. Shen, J. Zhai, *Appl. Phys. Lett.* **2015**, *107*, 032907.
[130] X. Zhang, Y. Shen, Q. Zhang, L. Gu, Y. Hu, J. Du, Y. Lin, C.-W. Nan, *Adv. Mater.* **2015**, *27*, 819.
[131] X. Zhang, Y. Shen, B. Xu, Q. Zhang, L. Gu, J. Jiang, J. Ma, Y. Lin, C.-W. Nan, *Adv. Mater.* **2016**, *28*, 2055.
[132] Y. Shen, J. Du, X. Zhang, X. Huang, Y. Song, H. Wu, Y. Lin, M. Li, C.-W. Nan, *Mater. Express* **2016**, *6*, 277.
[133] V. Tomer, E. Manias, C. Randall, *J. Appl. Phys.* **2011**, *110*, 044107.
[134] C. R. Dean, A. F. Young, I. Meric, C. Lee, L. Wang, S. Sorgenfrei, K. Watanabe, T. Taniguchi, P. Kim, K. L. Shepard, *Nat. Nanotechnol.* **2010**, *5*, 722.
[135] C. Sevik, A. Kinaci, J. B. Haskins, T. Çağın, *Phys. Rev. B* **2011**, *84*, 085409.
[136] Z. M. Dang, M. S. Zheng, J. W. Zha, *Small* **2016**, *12*, 1688.
[137] L. Yue, G. Pircheraghi, S. A. Monemian, I. Manas-Zloczower, *Carbon* **2014**, *78*, 268.
[138] Z.-M. Dang, H.-Y. Wang, B. Peng, C.-W. Nan, *J. Electroceram.* **2008**, *21*, 381.
[139] K. Yu, Y. Bai, Y. Zhou, Y. Niu, H. Wang, *Appl. Phys. Lett.* **2014**, *104*, 082904.
[140] S. Cho, J. S. Lee, J. Jang, *ACS Appl. Mater. Interfaces* **2015**, *7*, 9668.
[141] Y. Jin, N. Xia, R. A. Gerhardt, *Nano Energy* **2016**, *30*, 407.
[142] S. Luo, Y. Shen, S. Yu, Y. Wan, W.-H. Liao, R. Sun, C.-P. Wong, *Energ. Environ. Sci.* **2017**, *10*, 137.
[143] V. Tomer, C. Randall, G. Polizos, J. Kostelnick, E. Manias, *J. Appl. Phys.* **2008**, *103*, 034115.
[144] A. Azizi, M. R. Gadinski, Q. Li, M. A. AlSaud, J. Wang, Y. Wang, B. Wang, F. Liu, L.-Q. Chen, N. Alem, Q. Wang, *Adv. Mater.* **2017**, 1701864.
[145] G. Zhang, X. Zhang, H. Huang, J. Wang, Q. Li, L.-Q. Chen, Q. Wang, *Adv. Mater.* **2016**, *28*, 4811.
[146] B. Li, P. I. Xidas, K. S. Triantafyllidis, E. Manias, *Appl. Phys. Lett.* **2017**, *111*, 082906.
[147] H. Tang, Y. Lin, H. A. Sodano, *Adv. Energy Mater.* **2012**, *2*, 469.
[148] B. Xie, H. Zhang, Q. Zhang, J. Zang, C. Yang, Q. Wang, M.-Y. Li, S. Jiang, *J. Mater. Chem. A* **2017**, *5*, 6070.
[149] L. Yao, Z. Pan, S. Liu, J. Zhai, H. H. Chen, *ACS Appl. Mater. Interfaces* **2016**, *8*, 26343.
[150] L. Yao, Z. Pan, J. Zhai, H. H. Chen, *Nanoscale* **2017**, *9*, 4255.
[151] E. Baer, L. Zhu, *Macromolecules* **2017**, *50*, 2239.
[152] M. Mackey, D. E. Schuele, L. Zhu, L. Flandin, M. A. Wolak, J. S. Shirk, A. Hiltner, E. Baer, *Macromolecules* **2012**, *45*, 1954.

[153] K. Yin, Z. Zhou, D. E. Schuele, M. Wolak, L. Zhu, E. Baer, *ACS Appl. Mater. Interfaces* **2016**, *8*, 13555.
[154] L. Yao, D. Wang, P. Hu, B. Z. Han, Z. M. Dang, *Adv. Mater. Interfaces* **2016**, 201600016.
[155] M. A. Vecchio, Z. Ounaies, M. T. Lanagan, A. B. Meddeb, *IEEE Conf. Electr. Insul. Dielectr. Phenomena (CEIDP)* **2016**, 457.
[156] P. Hu, Y. Shen, Y. Guan, X. Zhang, Y. Lin, Q. M. Zhang, C.-W. Nan, *Adv. Funct. Mater.* **2014**, *24*, 3172.
[157] Y. Shen, Y. Hu, W. Chen, J. Wang, Y. Guan, J. Du, X. Zhang, J. Ma, M. Li, Y. Lin, L.-Q. Chen, C.-W. Nan, *Nano Energy* **2015**, *18*, 176.
[158] Y. Wang, J. Cui, Q. Yuan, Y. Niu, Y. Bai, H. Wang, *Adv. Mater.* **2015**, *27*, 6658.
[159] Y. Wang, J. Cui, L. Wang, Q. Yuan, Y. Niu, J. Chen, Q. Wang, H. Wang, *J. Mater. Chem. A* **2017**, *5*, 4710.
[160] Y. Wang, L. Wang, Q. Yuan, Y. Niu, J. Chen, Q. Wang, H. Wang, *J. Mater. Chem. A* **2017**, *5*, 10849.
[161] F. Liu, Q. Li, J. Cui, Z. Li, G. Yang, Y. Liu, L. Dong, C. Xiong, H. Wang, Q. Wang, *Adv. Funct. Mater.* **2017**, 1606292.
[162] Z. Pan, B. Liu, J. Zhai, L. Yao, K. Yang, B. Shen, *Nano Energy* **2017**, *40*, 587.
[163] G. Zhang, X. Zhang, T. Yang, Q. Li, L.-Q. Chen, S. Jiang, Q. Wang, *ACS Nano* **2015**, *9*, 7164.
[164] Z.-H. Shen, J.-J. Wang, Y. Lin, C.-W. Nan, L.-Q. Chen, Y. Shen, *Adv. Mater.* **2017**, 1704380.

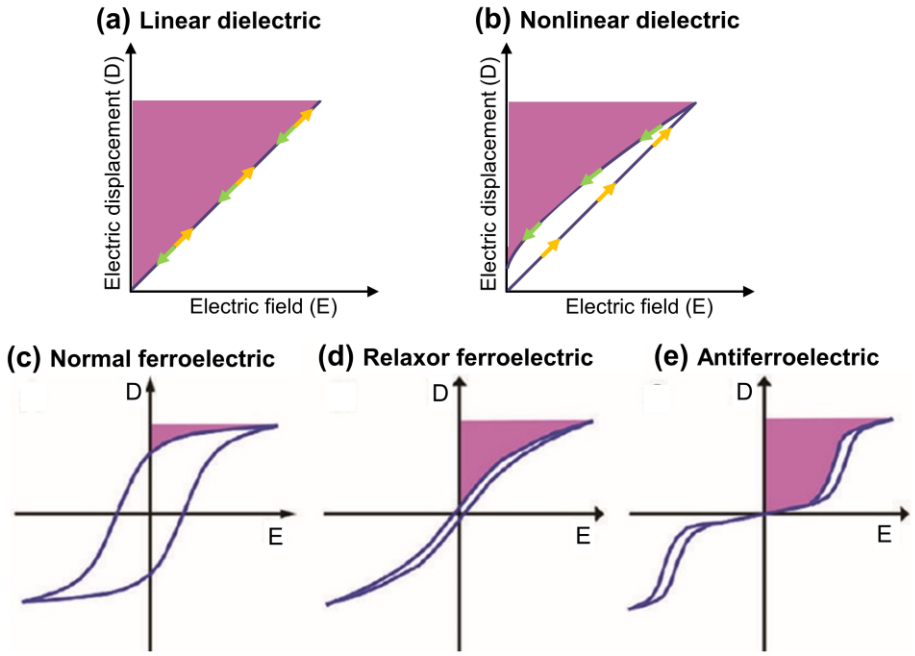

Figure 1. Schematic illustrations of *D*–*E* hysteresis loops: (a) unipolar for linear dielectrics. (b) unipolar for nonlinear dielectrics. (c) bipolar for normal ferroelectric

behavior. (d) bipolar for relaxor ferroelectric behavior. (e) bipolar for antiferroelectric behavior. Reproduced with permission.[34] Copyright 2012, American Chemical Society.

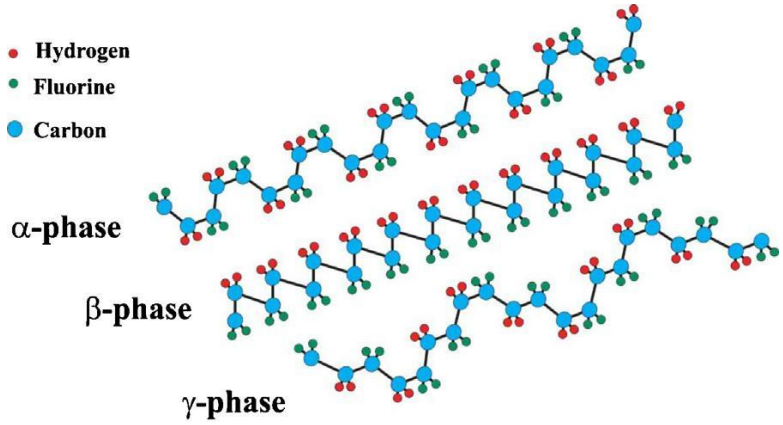

Figure 2. Schematic illustrations of chain conformation for α-, β-, and γ-phases of PVDF. Reproduced with permission.[39] Copyright 2014, Elsevier Ltd.

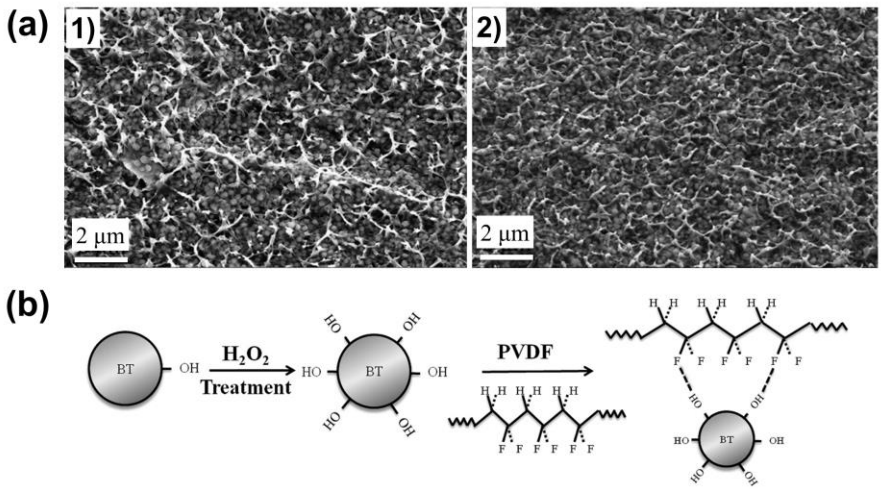

Figure 3. (a) Cross-sectional SEM images of the 1) PVDF/c-BT and 2) PVDF/h-BT nanocomposites with the filler content of 30 vol%. (b) Schematic illustration of the hydroxylation of BT nanoparticles and the formation of hydrogen bonds in PVDF/h-BT nanocomposites. Reproduced with permission.[84] Copyright 2011, American Chemical Society.

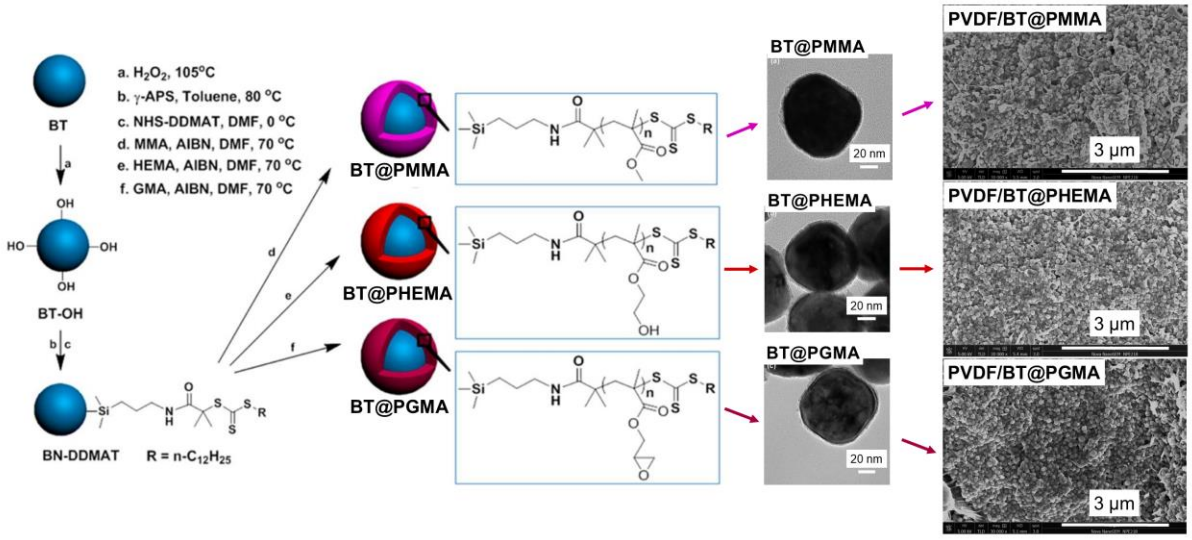

Figure 4. Schematic illustrations of the preparation process of the BT@polymer nanoparticles by surface-initiated RAFT polymerization, TEM images of BT@PMMA, BT@PHEMA and BT@PGMA and cross-sectional SEM images of PVDF/BT@PMMA, PVDF/BT@PHEMA and PVDF/BT@PGMA nanocomposites with the filler content of 20 vol%. Reproduced with permission.[113] Copyright 2014, American Chemical Society.

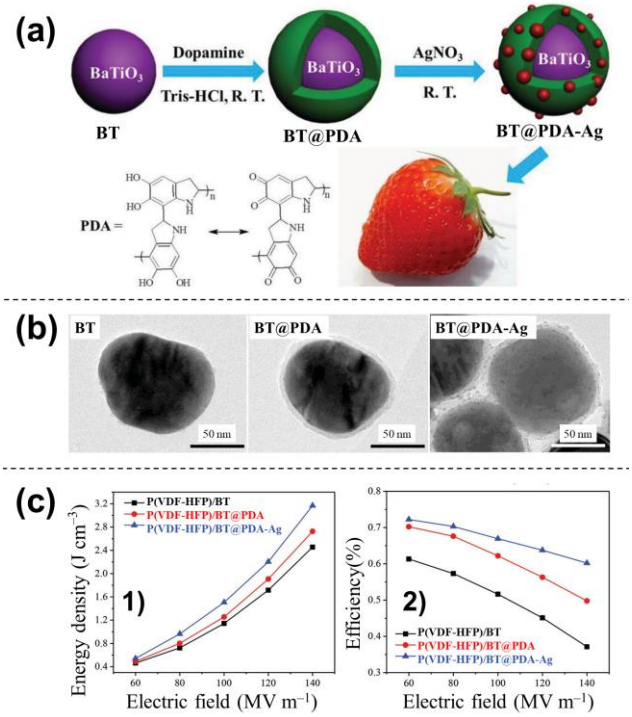

Figure 5. (a) Schematic illustration of the preparation of strawberry-like BT@PDA-Ag hybrid nanoparticle. (b) TEM images of the as-received BT, BT@PDA, and BT@PDA-Ag nanoparticles. (c) The energy density and the charge–discharge efficiency of the P(VDF-HFP)-based nanocomposites with as-received BT, BT@PDA, and BT@PDA-

Ag nanoparticles with the filler content of 20 vol%. The feed ratio of Ag^+ to BT@PDA nanoparticles is 2 wt%. Reproduced with permission.[117] Copyright 2015, Wiley-VCH.

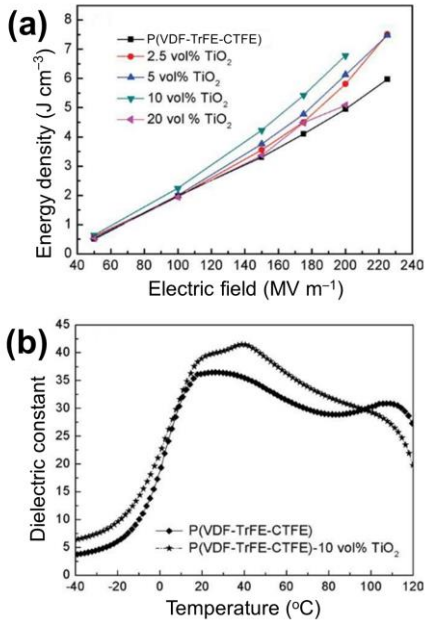

Figure 6. (a) The energy density of the pristine P(VDF-TrFE-CTFE) and nanocomposites as a function of the applied electric field. (b) Temperature dependence of the dielectric constant (*K*) of the pristine P(VDF-TrFE-CTFE) and the nanocomposite with 10 vol% TiO_2 measured at 1 kHz. Reproduced with permission.[30] Copyright 2009, Wiley-VCH.

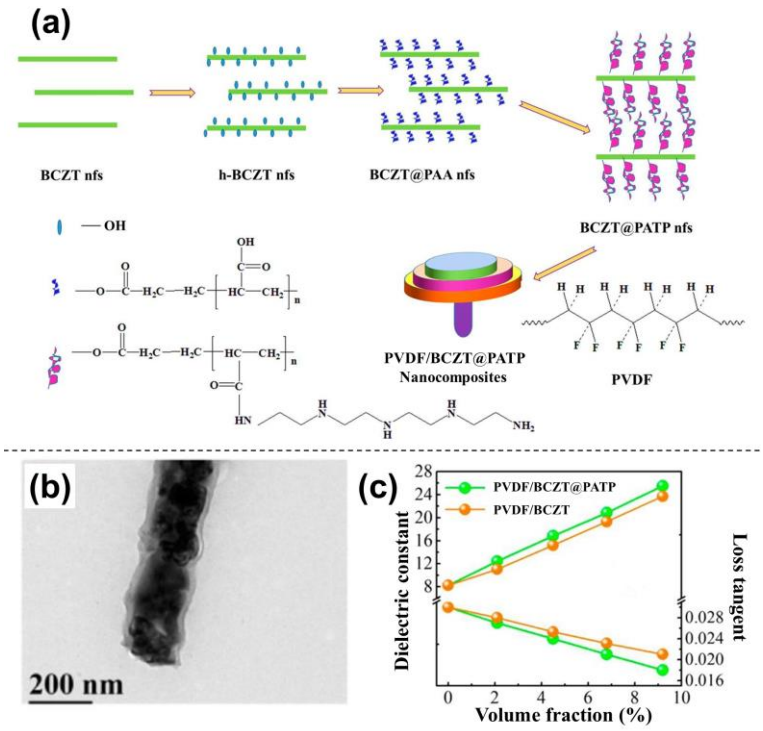

Figure 7. (a) Schematic illustration of the fabrication of BCZT@PATP nanofibers and the nanocomposite processes. (b) TEM image of the BCZT@PATP nanofiber. (c) Frequency dependence of the dielectric constant (*K*) and the dielectric loss tangent of PVDF/BCZT@PATP and PVDF/BCZT nanocomposites with varied volume fractions measured at 1 kHz. Reproduced with permission.[127] Copyright 2017, American Chemical Society.

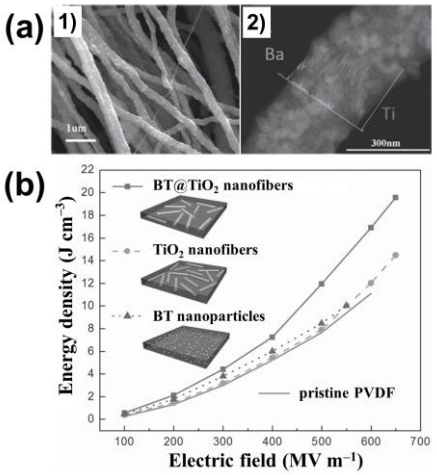

Figure 8. (a) 1) SEM image and 2) elements mapping image of BT@TiO_2 nanofiber. (b) The energy density of PVDF nanocomposites embedded with BT@TiO_2 nanofibers, TiO_2 nanofibers, BT nanoparticles, and pristine PVDF films as a function of electric field, the filler content of the three nano-inclusions are fixed at 3 vol%. Reproduced with permission.[130] Copyright 2014, Wiley-VCH.

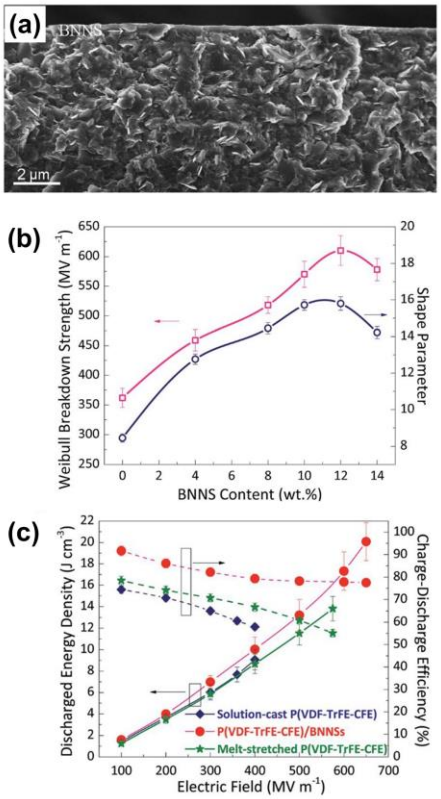

Figure 9. (a) Cross-sectional SEM image of the P(VDF-TrFE-CFE)/BNNS composite film with 12 wt% BNNSs. (b) Weibull breakdown strength (scale parameter) and shape parameter as functions of BNNS fraction. (c) Comparison of discharged energy density and charge–discharge efficiency of pristine P(VDF-TrFE-CFE) and P(VDF-TrFE-CFE)/BNNSs nanocomposite with 12 wt% of BNNSs at different electric fields. Reproduced with permission.[37] Copyright 2015, The Royal Society of Chemistry.

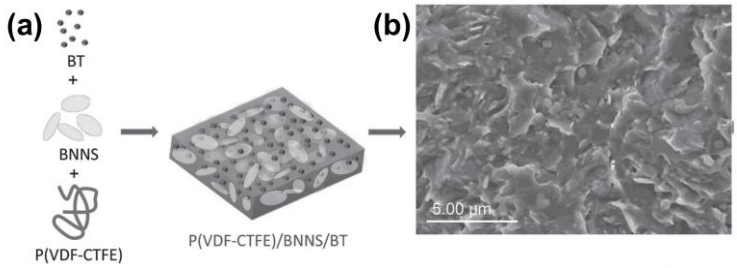

Figure 10. (a) Schematic illustration of P(VDF-CTFE)-based ternary nanocomposite film containing both BT and BNNS. (b) Cross-sectional SEM images of P(VDF-CTFE)/BNNS/BT ternary nanocomposite film with 12 wt% BNNSs and 15 wt% BT. Reproduced with permission.[24] Copyright 2014, Wiley-VCH.

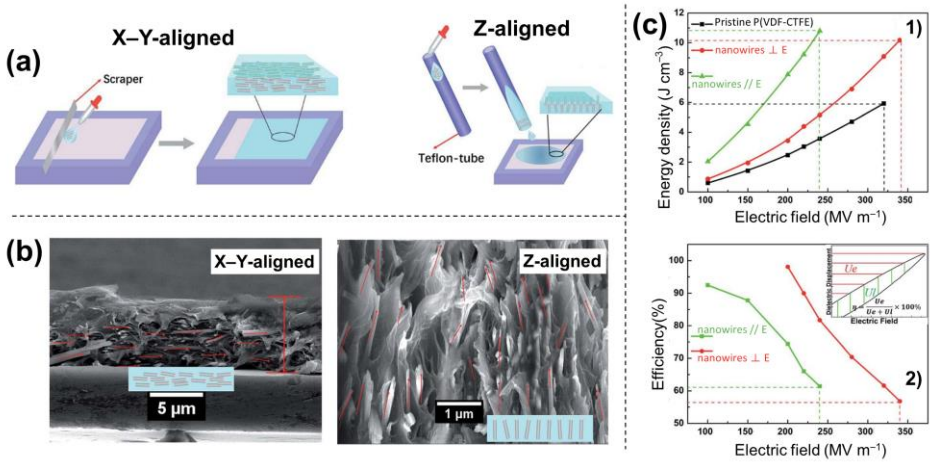

Figure 11. (a) Schematic illustration of the preparation process of the X–Y-aligned and the Z-aligned nanocomposites. (b) Representative cross-sectional SEM images of the X–Y-aligned and the Z-aligned nanocomposite film. (c) 1) variations of discharged energy densities and 2) charge–discharge efficiencies of pristine P(VDF-CTFE), X–Y-aligned (BT nanowires ⊥ E) and Z-aligned (BT nanowires // E) nanocomposites. Reproduced with permission.[148] Copyright 2017, The Royal Society of Chemistry.

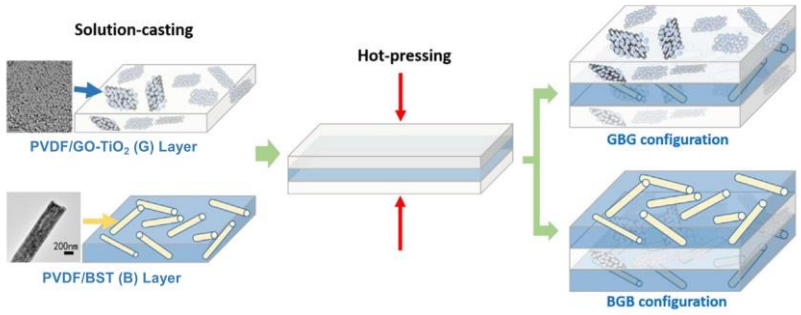

Figure 12. Schematic illustrations of the preparation and configurations of the sandwich-structured polymer nanocomposites. PVDF/GO-TiO_2 (G) layer and PVDF/BST nanofibers (B) layer are cast from solution and subjected to hot-pressing to form polymer nanocomposites of two configurations, i.e., GBG & BGB. Reproduced with permission.[157] Copyright 2015, Elsevier Ltd.

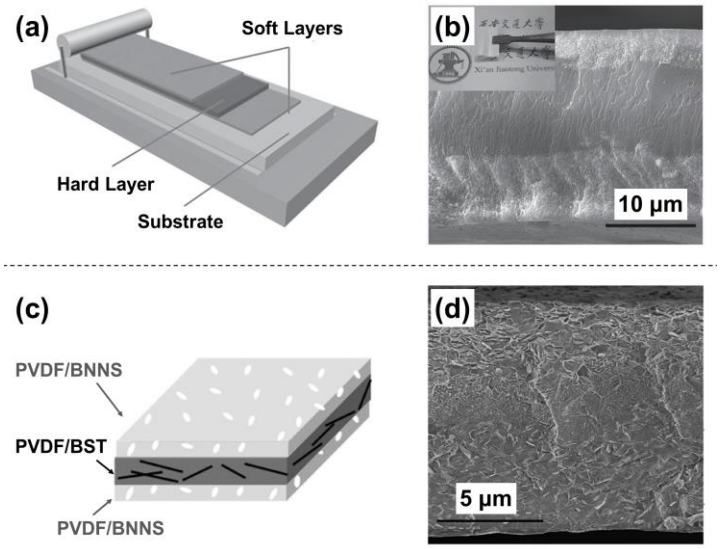

Figure 13. (a) Schematic illustration of the fabrication process of sandwich-structured PVDF/BT nanocomposites. (b) Cross-sectional SEM image of sandwich-structured PVDF/BT nanocomposite with 20 vol% BT in "soft layers." Inset: Photograph of the sandwich-structured PVDF/BT nanocomposite. Reproduced with permission.[158] Copyright 2015, Wiley-VCH. (c) Schematic illustration of the sandwich-structured film composed of PVDF/BNNSs as outer layers and PVDF/BST as the central layer. (d) Cross-sectional SEM image of sandwich-structured nanocomposite with 10 vol% BNNS in the outer layers and 8 vol% BST nanowires in the central layer. Reproduced with permission.[161] Copyright 2017, Wiley-VCH.

He Li is currently a graduate student majoring in Electrical Engineering at Xi'an Jiaotong University and a jointly advised student in the Department of Materials Science and Engineering at The Pennsylvania State University, University Park. His research interests focus on dielectric polymers and polymer nanocomposites for capacitive energy storage, the interface effects in complex high voltage insulation systems.

Zongren Peng is a Professor of Electrical Engineering at Xi'an Jiaotong University. He graduated from Xi'an Jiaotong University in 1977. His research interests lie in the calculation and optimization of insulation structures for ultra-high voltage power equipment, the forming mechanisms and measurement of space charge in dielectrics, and the interface effects in complex high voltage insulation systems.

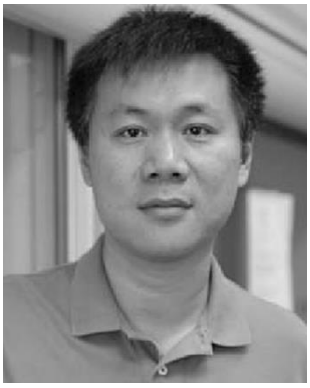

Qing Wang is a Professor of Materials Science and Engineering at The Pennsylvania State University, University Park. He received his Ph.D. in 2000 from The University of Chicago. Prior to joining the faculty at Penn State in 2002, he was a postdoctoral fellow at Cornell University. His research programs are centered on development of novel functional polymers and polymer nanocomposites with unique dielectric, electronic, and transport properties for applications in energy storage and harvesting.

The introduction of nanostructured inorganic fillers into ferroelectric polymers represents an emerging and promising approach to dielectric materials with high energy densities for capacitive energy storage. The most recent advances in the design and preparation of the ferroelectric polymer nanocomposites are summarized. The comprehensive impacts of nanofillers on the dielectric properties and capacitive performance of the composites are reviewed.

Keyword: Ferroelectric Polymers, Nanocomposites, Inorganic Nanostructures, Energy Storage, Capacitors,

H. Li, F. Liu, B. Fan, D. Ai, Z. Peng, Q. Wang*

Nanostructured Ferroelectric Polymer Composites for Capacitive Energy Storage

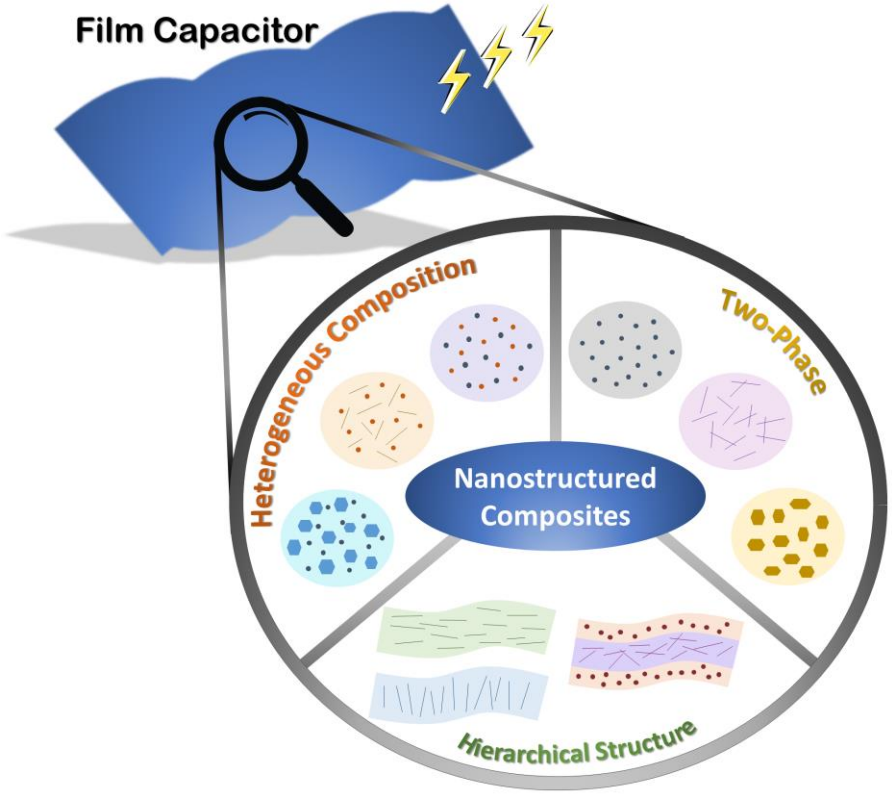
Film Capacitor
Heterogeneous Composition
Two-Phase
Nanostructured Composites
Hierarchical Structure